

## Use Authorization

In presenting this thesis in partial fulfillment of the requirements for an advanced degree at Idaho State University, I agree that the Library shall make it freely available for inspection. I further state that permission to download and/or print my thesis for scholarly purposes may be granted by the Dean of the Graduate School, Dean of my academic division, or by the University Librarian. It is understood that any copying or publication of this thesis for financial gain shall not be allowed without my written permission.

Signature \_\_\_\_\_

Date \_\_\_\_\_

# **Decoloration of Rhodamine B Through Hydrodynamic Cavitation: Degradation Kinetics**

by  
Tianyu Han

A thesis  
submitted in partial fulfillment  
of the requirements for a degree of  
Master of Science in Environmental Science and Management  
Idaho State University  
Fall 2015

Copyright (2015) Tianyu Han

To the Graduate Faculty:

The members of the committee appointed to examine the thesis of TIANYU HAN find it satisfactory and recommend that it be accepted.

---

Chikashi Sato Ph.D.,  
Major Advisor

---

Jeffrey J. Rosentreter Ph.D.,  
Secondary Advisor

---

Michael McCurry Ph.D.,  
Graduate Faculty Representative

## Acknowledgements

Foremost, I would like to express my sincere gratitude to my advisor Dr. Sato for the continuous support of my graduate study and research, for his patience, motivation, enthusiasm, and immense knowledge. His guidance helped me in all the time of research and writing of this thesis. I could not have imagined having a better advisor and mentor for my graduate study.

Besides my advisor, I would like to thank Dr. Rosentreter, my secondary advisor, and Dr. McCurry, for their encouragement and insightful comments.

My sincere thanks also goes to senior design team Fadi Alalkam, Mark Hayes, Grayden Howard, Robert Smith, with their nicely design, I was able to run my experiments.

I thank my lab-mates: Tulio Porto and Sukriti Panthi for the helping of running AC experiments. Also I thank my friends in Idaho State University: Yibing Fan, Yingying Lu, Yao Zhang, Xiang Gao, Sneha Suresh, Maedeh Mozned for their support and encouragement.

Last but not the least, I would like to thank my parents Xiao Han and Caihua Wu, for giving birth to me at the first place and supporting me spiritually throughout my life.

# TABLE OF CONTENTS

<b>LIST OF FIGURES.....</b>	<b>viii</b>
<b>LIST OF TABLES.....</b>	<b>ix</b>
<b>Abstract .....</b>	<b>x</b>
<b>Chapter 1: Introduction .....</b>	<b>1</b>
<b>1.1 Background .....</b>	<b>1</b>
<b>1.2 Objectives.....</b>	<b>4</b>
<b>Chapter 2: Literature Review.....</b>	<b>6</b>
<b>2.1 Treatment Processes for Dye-Contained Wastewater.....</b>	<b>6</b>
<b>2.1.1 Biological Treatment.....</b>	<b>6</b>
<b>2.1.2 Chemical Treatment .....</b>	<b>7</b>
a. Coagulation.....	7
b. Electrocoagulation .....	8
<b>2.1.3 Advanced Oxidation Processes.....</b>	<b>8</b>
a. Fenton Oxidation.....	9
b. Ozone Oxidation.....	10
c. Electrochemical Oxidation .....	10
d. Photochemical Oxidation .....	11
<b>2.2 Application of Cavitation in Wastewater Treatment.....</b>	<b>12</b>
<b>2.2.1 Acoustic Cavitation.....</b>	<b>13</b>
<b>2.2.2 Hydrodynamic Cavitation.....</b>	<b>14</b>
a. Orifice Plate.....	14
b. Venturi Tube.....	17
c. Other Cavitation Methods.....	18
<b>Chapter 3: Experimental.....</b>	<b>20</b>
<b>3.1 Materials.....</b>	<b>20</b>
<b>3.2 Experimental Setup .....</b>	<b>21</b>
3.2.1 HC System Setup.....	21
3.2.2 AC System Setup.....	24
<b>3.3 Experimental Procedures .....</b>	<b>25</b>
3.3.1 HC System.....	25
3.3.2 AC System.....	26
<b>3.4 Analysis.....</b>	<b>26</b>
<b>Chapter 4: Results and Discussion .....</b>	<b>27</b>
<b>4.1 Preliminary Study .....</b>	<b>27</b>
<b>4.2 Degradation Kinetics .....</b>	<b>29</b>
<b>4.3 Effect of Dye Concentration .....</b>	<b>31</b>
<b>4.4 Dye Solution pH.....</b>	<b>33</b>
<b>4.5 Comparison of Two Venturi Tubes .....</b>	<b>35</b>
<b>4.6 Effect of Inlet Pressure .....</b>	<b>36</b>
<b>4.7 Comparison of Energy Efficiency between HC and USUV System.....</b>	<b>39</b>
<b>Chapter 5: Conclusion.....</b>	<b>42</b>
<b>References .....</b>	<b>43</b>

<b>Appendix A. UV-vis-spectrophotometer Calibration.....</b>	<b>48</b>
<b>A-1. Preparation of Rhodamine B Standard Solutions.....</b>	<b>48</b>
<b>A-2. Calibration of UV Spectrophotometer.....</b>	<b>49</b>
<b>A-3. Measurement of Samples.....</b>	<b>49</b>
<b>A-4. Standard Curve.....</b>	<b>50</b>
<b>Appendix B. Original Data.....</b>	<b>54</b>
<b>B-1. Original Data of Preliminary Study.....</b>	<b>54</b>
<b>B-2. Original Data for two Venturi tubes.....</b>	<b>55</b>
<b>B-3. Original Data of AC System.....</b>	<b>61</b>
<b>Appendix C. Calculation.....</b>	<b>63</b>
<b>C-1. Degradation Rate Constant of HC System.....</b>	<b>63</b>
<b>C-2. Degradation Rate Constant of AC System.....</b>	<b>63</b>
<b>C-3. Removal Efficiency.....</b>	<b>64</b>
<b>C-4. Energy Efficiency Calculation of HC and AC processes.....</b>	<b>64</b>

## LIST OF FIGURES

Fig. 2-1 Sketch of combined chamber and swirling cavitation chamber (Wang, et al., 2008).....	18
Fig. 3-1 Structural formula of rhodamine B (Yikrazuul, 2008; Jain, et al., 2007) .....	20
Fig. 3-2 Schematic representation of the hydrodynamic cavitation system .....	22
Fig. 3-3 Hydrodynamic cavitation system (Shot by senior design team-Alalkam, Hayes, Howard, Smith).....	22
Fig. 3-4 The schematic cavitation devices.....	23
Fig. 3-5 Schematic representation of the acoustic cavitation system .....	25
Fig. 4-1 Degradation of rhodamine B with Venturi tube #1 (Model 283) with inlet pressure of 70 psi (0.483 MPa) and initial dye concentration of $1.20 \times 10^{-2}$ mM: (a) zeroth-order kinetics; (b) first-order kinetics.....	29
Fig. 4-2 Degradation of rhodamine B with the Venturi tube #2 (Model 287) with inlet pressure of 50 psi (0.344 MPa) and initial dye concentration of $1.20 \times 10^{-2}$ mM: (a) zeroth-order kinetics; (b) first-order kinetics.....	30
Fig. 4-3 First order degradation of rhodamine B with Venturi tube #1 (Model 283) with inlet pressure of 70 psi (0.483 MPa) and two different initial concentrations of dye: $1.20 \times 10^{-2}$ mM and $2.51 \times 10^{-3}$ mM.....	32
Fig. 4-4. Hydrogen-ion activity of dye solution through HC process with Venturi tube #1 (Model 283): inlet pressure 70 psi, initial concentration $2.51 \times 10^{-3}$ mM ( $\{H^+\} = 10$ -pH mM).....	34
Fig. 4-5. Hydrogen-ion activity of dye solution through HC process with Venturi tube #1 (Model 283): inlet pressure 70 psi, initial concentration $1.20 \times 10^{-2}$ mM ( $\{H^+\} = 10$ -pH mM).....	34
Fig. 4-6. Hydrogen-ion activity of dye solution through HC process with Venturi tube #2 (Model 287): inlet pressure 50 psi, initial concentration $1.20 \times 10^{-2}$ mM ( $\{H^+\} = 10$ -pH mM).....	35
Fig. 4-7 Degradation rate constant of rhodamine B at different inlet pressure: Venturi tube #2 (Model 287), initial concentration $1.20 \times 10^{-2}$ mM.....	39
Fig. 4-8 Comparison of Energy Efficiency between HC and USUV System .....	40
Fig. A-4.1 Calibration curve developed for low initial concentration HC experiments. ....	51
Fig. A-4.2 Calibration curve developed for high initial concentration HC experiments.....	51
Fig. A-4.3 Calibration curve developed for AC system .....	52

## LIST OF TABLES

Table 2-1 Cavitation device information .....	24
Table 4-1 Preliminary study of cavitation devices .....	28
Table 4-2 Reaction kinetics with various cavitation devices and compounds .....	31
Table 4-3 Summary of experimental results of Venturi tubes (Model 283 and Model 287) .....	36
Table 4-4 Summary of experiment data for different inlet pressure .....	38
Table 4-5 Summary of HC and US system .....	39
Table A-1.1 Rhodamine B standard solution for low initial concentration experiment.....	48
Table A-1.2 Rhodamine B standard solution for high initial concentration experiment.....	48
Table A-4.1 Standard solution and its absorbance.....	50
Table A-4.2 Standard solution and its absorbance.....	51
Table A-4.3 Standard solution and its absorbance.....	52

## Abstract

Hydrodynamic cavitation (HC) was investigated as a potential application to the treatment of industrial wastewater containing rhodamine B dye. Using a pilot-scale, continuous recirculating flow system, the degradation rates of rhodamine B were determined for various cavitation devices (i.e., orifice plates, Venturi tubes, and needle tubes) with various physical and chemical conditions: *i*) initial concentration of the dye, *ii*) dye solution pH, and *iii*) inlet pressure of the cavitation devices. Results showed that, among the devices tested, the most effective HC device was Venturi tube #2 (Model 287) with the highest dye removal efficiency of 10.33 % , first-order degradation rate constant of  $1.09 \times 10^{-3} \text{ min}^{-1}$  at the initial rhodamine B concentration of  $8.74 \times 10^{-3} \text{ mM}$  and inlet pressure of 50 psi (0.345 MPa). The HC system with Venturi tube #2 (Model 287) was about 10% more energy efficient than the acoustic cavitation system studied in this work.

# Chapter 1: Introduction

## 1.1 Background

The increasing demand for colored fabrics and a large market for textile industries around the world pose a serious threat to our environment. Because of the use of dyes as a main raw material, its environmental impact has been concerned by the society. In order to provide customers with a long lasting and continued fashion appeal of garments, dyes are synthesized to resist to the natural weathering: Therefore dye materials must be physically, chemically and biologically stable (Boyter, 2007). These properties mean it is naturally nondegradable and it could stay in nature for a long time. The color in the water will block the light to enter and prohibit photosynthesis of aquatic plants and further can cause the death of aquatic animals. Directly exposing to high concentration of fluorescein dye could lead to a mortality of fish (Taylor and Hanson, 2010): Pouliquen et al. (1995) noted an LD<sub>50</sub> of fluorescein is about 1,000 ppm in turbot after 96 hours. All these properties, however, attribute to serious environmental hazards.

A large volume of textile productions results in the generation of enormous quantities of tainted wastewater. In 2014, more than 1 million tons of dyes are on the market. Over 1 million tons of dyes are continuingly produced every year; of which about one-half are used for dyes production (Arora, 2014). Up to 0.2 million tons of textile dyes are estimated to be lost to effluents every year in the dyeing and finishing processes, as a result of inefficient dyeing processes (Ogugbue and Sawidis, 2011).

Most of the dye compounds are visible in natural water at the concentrations as low as 1 ppm. The dye concentrations in textile processing wastewater usually range

from 10 to 200 ppm (Kumar, 2014). The presence of dye in this range could harm the environment, as it reduces water transparency and decreases the solubility of oxygen in the water, in addition to causing aesthetic damages. The dye absorbs and reflects the sunlight entering a water column. Sunlight is essential in an aqueous ecosystem, as it is the energy source for the primary producers in the food web. Interference of sunlight entering the ecosystem affects the growth of algae and other photosynthetic organisms. Consequently, reduced light energy impacts on the growth of larger species. To make matters worse, certain types of dyes can bioaccumulate in aquatic organisms, potentially posing risks to human health (Pereira and Alves, 2012). The legislations that regulate the dye in industrial effluents are increasingly stringent. Such legislations have passed and enacted in not only developed countries but also developing countries (Robinson et al., 2001). Enforcement of the environmental laws to textile industries ensures that the textile factories pretreat their wastewater on-site to meet the regulatory requirements, prior to discharging it to municipal wastewater treatment facilities.

The discharge of the rhodamine B dye in the water environment has drawn a considerable attention by aquatic ecology scientists in the field of aquatic ecology. Rhodamine B (a xanthene class red dye) is widely used by textile manufacturers as a colorant (Merouani et al., 2010). Rhodamine B is potentially carcinogenic, harmful to human eyes, and toxic to aquatic organisms (Jain et al., 2007). Due to its toxic and harmful effects on human beings and the environment, rodamine B is listed in the following U.S. regulatory documents:

- California Occupational Safety and Health Regulations (CAL/OSHA) – Hazardous Substances List;

- California Proposition 65 – Carcinogens;
- California Proposition 65 – Priority List for the Development of NSRLs for Carcinogens;
- Maine Chemicals of High Concern List;
- New Jersey Right to Know Hazardous Substances;
- Pennsylvania – Hazardous Substance List;
- DOE Temporary Emergency Exposure Limits (TEELs);
- EPCRA Section 313 Chemical List;
- FDA CFSAN Color Additive Status List;
- List of Lists – Consolidated List of Chemicals Subject to the Emergency Planning and Community Right-to-Know Act (EPCRA) and Section 112(r) of the Clean Air Act;
- Toxic Substances Control Act (TSCA) - Inventory

Conventional water and wastewater treatment methods including biological treatment, adsorption, and coagulation-flocculation have been investigated to remove dye compounds from water and wastewater (EPA, 1978; Bailey et al., 1999). Because most of the dye compounds are highly biorefractory and often toxic, the conventional biological processes (activated sludge) have not only failed to degrade such compounds, but also have caused inactivation of microorganisms in bioreactors (an activated sludge aeration tank). In the coagulation-flocculation and adsorption processes, dye contaminants are transferred from a liquid phase to a solid phase. After the treatment, therefore, the contaminants still exist in the solid phase, requiring safe final disposal methods for the solid wastes (Gore et al., 2014)

Advanced Oxidation Processes (AOPs) involve an in-situ production of hydroxyl radicals ( $\bullet\text{OH}$ ). Having the oxidation potential of 2.8 V,  $\bullet\text{OH}$  is the strongest oxidizing agent after fluorine. Because  $\bullet\text{OH}$  is capable of oxidizing biorefractory contaminants in water, the AOPs have drawn many scientists and engineers' attention in recent years (Adewuyi, 2005). Although various AOP technologies such as Fenton oxidation, ozonation, electrochemical oxidation and photochemical oxidation have been investigated in laboratories, these AOPs have not been implemented in industries due to high cost and design constraints.

The cavitation technique can also be considered as an AOP, as it has the capacity to generate  $\bullet\text{OH}$  in water. Cavitation is a phenomenon that involves formation, growth, and collapse of micro- or nano-bubbles. The cavitation bubbles can be created in a dynamic flow with a sudden pressure change and subsequent recovery (Gogate and Pandit, 2001). In the past, most cavitation research focused on acoustic cavitation (AC). However, a large energy requirement makes the acoustic process impractical in large-scale applications. Compared to AC, the hydrodynamic cavitation (HC) process can be cost-effective and easy to scale up for practical applications (Gore et al., 2014).

## 1.2 Objectives

The objectives of this study are:

- 1) To design and build a pilot-scale water treatment system that uses hydrodynamic cavitation (HC);
- 2) To examine the degradation kinetics of rhodamine B dye with various devices that can potentially generate HC;

- 3) To improve the degradation efficiency of rhodamine B dye by varying treatment conditions.

## **Chapter 2: Literature Review**

### **2.1 Treatment Processes for Dye-Contained Wastewater**

Large quantities of colored wastewater discharged by textile industries have raised serious environmental concerns. Dyes used in textile industries can have acute and chronic effects on not only human health but also environmental health. The dye can be visible even at trace levels in water. When the concentration of dye exceeds a certain level, sunlight entering the water is blocked. Consequently, the photosynthetic activities of aquatic organisms can be interfered or inhibited, resulting in destruction of the ecosystem.

#### **2.1.1 Biological Treatment**

In the past decades, numerous studies have been conducted aiming to explore a cost-effective method to decolorize dye-containing wastewater. A conventional biological treatment technique has been employed to treat wastewater containing dye chemicals (EPA, 1978; Kandelbuer, Cavaco-paulo and Gubitz, 2007). The biological wastewater treatment techniques are generally divided into aerobic, anaerobic, and anoxic methods.

The aerobic processes treat polluted water with the help of aerobic and facultative microorganisms. The anaerobic and anoxic processes use anaerobic and facultative bacteria, respectively, in the wastewater treatment systems. Based on the media employed in the processes, the biological treatment can be divided into two major groups: the suspended growth system (e.g., active sludge) and the attached growth or biofilm

processes (e.g., trickling filter). The biological treatment is a low-cost technique; however, there are major drawbacks: the dyes are biorefractory and often toxic. Furthermore, intermediate products produced during the biodegradation of the dyes can be toxic to the microorganism themselves, resulting in a failure of the treatment processes (Wang et al., 2011b; Kandelbuer et al., 2007).

## **2.1.2 Chemical Treatment**

### ***a. Coagulation***

Coagulation is a conventional chemical treatment technique that deals with several water treatment concerns, including turbidity, color, taste, and odor. Coagulation uses chemical additives as coagulants reduce the electronic charge on the surface of suspended particles in the water or wastewater. The coagulate causes dirt particles to form larger, denser flocs and sink to the bottom of a clarifier (Wang et al., 2011b). A wide application of coagulation in the wastewater treatment systems can date back to 19<sup>th</sup> century. Nowadays, aluminum and iron salts are widely used as coagulants in primary wastewater treatment process with the advantage of relatively low market prices (Wang et al., 2011b).

Aluminum or iron salts have been used as coagulants for color removal purposes (Wang et al., 2011b). The mechanism of coagulation is based on the destabilization of colloids by reducing the net electrical repulsive forces at particle surfaces that keep them apart. Coagulants can provide opposite charges, which let the colloid particles overcome the repulsive charge on their surfaces, form larger particles, and being able to precipitate

under self-gravity. The process usually is very fast, taking seconds to complete (Davis and Cornwell, 2006).

Even though coagulation is a simple and efficient method to remove or reduce color, there are major disadvantages. First, this method is expensive: Large quantities of coagulant chemicals are required to meet the water quality standards; the chemicals, once used, cannot be recovered economically for reuse. Second, a large amount of chemical precipitates (sludge) must be disposed of: The disposal of toxic solid waste is problematic as it can introduce a secondary pollution to the environment (Hardin, 2007).

### ***b. Electrocoagulation***

Electrocoagulation is a novel coagulation method that has been practiced for industrial wastewater treatment in recent years. This process is developed based on the same mechanism of physicochemical coagulation. Other than adding chemicals to reduce the surface charge of suspended particles, passing electric current through assigned electrodes. In this process, highly charged metal oxide species (coagulants) are produced; thus, an over-feeding of chemicals (coagulants) can be avoided. This technique is widely used in industries to remove color from wastewater. However, the main disadvantage is a high electrical power input, which reduces the cost-effectiveness of the entire system (Hardin, 2007).

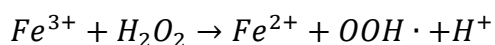
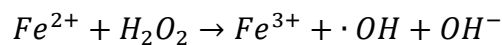
### **2.1.3 Advanced Oxidation Processes**

Advanced Oxidation Processes (AOPs) refers to the treatment methods to oxidize contaminants by hydroxyl radicals ( $\bullet\text{OH}$ ) generated by the processes (Glaze et al. 1987).

AOPs depend on an on-site production of •OH. Commonly, ozone (O<sub>3</sub>), hydrogen peroxide (H<sub>2</sub>O<sub>2</sub>), or Fenton reagents is employed to help generating •OH on site (National Water Research Institute, 2000). Having the capacity to reduce the concentration of contaminants from the ppm to ppb levels, AOPs are hailed as “water treatment processes of the 21st century” (Munter, 2001).

#### *a. Fenton Oxidation*

The Fenton reaction has attracted environmental engineers’ attention, as it produces hydroxyl radicals at low costs. Fenton’s reagent was found in the 1890s, and was suggested as a chemical additive in the industrial wastewater treatment processes in the 1930s (Fenton, 1894; Hardin, 2007). The reagent is a mixture of hydrogen peroxide (H<sub>2</sub>O<sub>2</sub>) and an iron salts (reduced iron such as Fe<sup>0</sup> and Fe<sup>2+</sup>). Oxidation of ferrous ion (Fe<sup>2+</sup>) to ferric ion (Fe<sup>3+</sup>) by H<sub>2</sub>O<sub>2</sub> generates •OH and Fe<sup>3+</sup>; Fe<sup>3+</sup> is then reduced to Fe<sup>2+</sup> by H<sub>2</sub>O<sub>2</sub> to form peroxide radical (OOH•) and hydrogen ion (H<sup>+</sup>) (Benatti and Tavares, 2012; Hardin, 2007).



As the chemical reactions proceed, the iron salt (act as a catalyst) is conserved and hydroxyl radicals are produced to attack various contaminants present in water. Xu et al. (2004) studied the degradation of 20 various dyes with the Fenton process. Results showed that the color removals of acidic, reactive, direct and cationic dyes were 87% to 100%. The color removals of disperse and vat dyes were between 30% and 56%. However, this process is restrained by various iron chelators, such as oxalic and citric,

EDTA and phosphates. The possibility of inactivation of the reagent has to be taken into account when it is applied to the industrial wastewater treatment (Hardin, 2007).

### ***b. Ozone Oxidation***

Ozone oxidation (Ozonation) is a powerful water decolorizing technique. Ozone has a very high oxidation potential (2.07 V), twice the oxidizing power of chlorine (Snoeyink and Jenkins, 1980). This property makes ozone oxidation an effective and fast decolorizing agent. Ozone can oxidize a non-biodegradable toxic compounds in the wastewater treatment processes, and improve bio-treatability of wastewater. The second superiority of ozonation technique is that the process does not increase either wastewater volumes or sludge mass. Ozone initiates and accelerates breaking of chemical bonds of compounds in wastewater effluents (Hardin, 2007). The main drawback of this method is a potential release of carcinogenic amines and other toxic byproducts (Lin and Chen, 1997).

### ***c. Electrochemical Oxidation***

The electrochemical technique has been studied for a textile wastewater treatment purpose in recent years. The main mechanism of the electro-oxidation process is transfer of electrons, in which the contaminants in water or wastewater can be destroyed through either a direct or indirect process. In a direct process, electrons generated by on site will attack the pollutants adsorbed on the anode. This process can degrade large, complex organic chemicals into small molecules. In an indirect process, strong oxidants (ozone, hydrogen peroxide, etc.) will be generated in-situ through electrochemical reactions. The pollutants are then destroyed through oxidation reactions. The advantage of this

technique is that it involves no secondary pollution, no additives needed, and easy operation. According to Nordin et al. (2013) and Wang et al. (2011), this technique is one of the main research directions in wastewater treatment of the future.

#### ***d. Photochemical Oxidation***

Photochemical oxidation is a novel advanced oxidation process. The mechanism of photochemical oxidation is the utilization of hydroxyl radicals generated by light energy. Depending on different applications, ultraviolet radiation, UV (with wavelengths ranging from 100 to 400 nm) or visible radiation (400 to 700 nm) is employed to produce •OH. Based on different principles, application purposes, and wavelength requirements, the photochemical oxidation technologies are broadly classified into four groups: vacuum UV photolysis, UV/oxidation processes, the photo-Fenton process, and sensitized advanced photochemical oxidation processes (US EPA, 1998). Kusic et al. (2006) investigated the degradation of Acid Orange 7 with the UV assisted photo-Fenton process. In their study, a complete decolorization was obtained at a constant temperature of 25 °C. Photochemical oxidation has the following significant advantages: *i*) it can be operated under a mild condition (ambient temperature and pressure); *ii*) it is highly energy efficient; and *iii*) it has the ability to degrade pollutants completely. The disadvantage is that the performance of photochemical oxidation process is not ideal for treating high concentration of pollutants in water or wastewater (Wang et al., 2011b).

## 2.2 Application of Cavitation in Wastewater Treatment

The physical phenomenon of the generation of micro- or nano-bubbles in water is called cavitation. The bubble collapses generated in this process are called cavities. Cavitation can occur in water as a result of a sudden pressure change in a dynamic flow. The formation of micro- or nano-bubbles can be conceived as an evidence of cavitation. A cavitation bubble releases tremendous energy as extremely high temperature (about 5000°C) and pressure (50-100 MPa) (Wu et al., 2007). This energy is sufficient enough to dissociate H<sub>2</sub>O to •OH and •H. The hydroxyl radicals are capable of oxidizing biorefractory contaminants in water and wastewater (Gogate and Pandit, 2001).

Cavitation relates the deterioration of water pipelines, hydraulic pumps, and flow control devices. The cavitation phenomenon was first observed on a ship propeller: the surface of the metal propeller was corroded (Leong et al., 2011; Thorneycroft and Barnaby, 1895). The generation of fine bubbles around the corroding area was the culprit for the damage of the ship propeller and water supply pumps. This phenomenon attracted scientists and engineers to develop new technologies, such as homogenization in the chemical engineering fields, the destruction of kidney stones in the biomedical field, and wastewater treatment in the environmental engineering field. The advantages of being chemical-free, low energy consumption, and easy scale-up attracted environmental engineers' attention to make this phenomenon into a practical wastewater treatment application.

Based on the modes of generation, cavitation can be divided into four types: acoustic (ultrasonic) cavitation, hydrodynamic cavitation (hydraulic power), optic cavitation and particle cavitation (Gogate and Pandit, 2001). Given abilities to generate

high intensity cavities (high temperature and pressure, shear forces, shock waves, and hydroxyl radicals) and easiness of operation, acoustic cavitation and hydrodynamic cavitation have been studied for industrial applications over the past decades (Gogate and Pandit, 2001; Sivakumar and Pandit, 2002).

### **2.2.1 Acoustic Cavitation**

Acoustic cavitation can be produced by ultrasonic irradiation in liquid. When liquid is irradiated with an appropriate-frequency of ultrasound, sound waves move through the liquid results in alternating high-pressure (compression) and low-pressure (rarefaction) cycles. The compression-rarefaction cycles eventually break the bonds between water molecules. The alternating rate depends on the frequency of the ultrasound (Mandal et al., 2015). Under a low-pressure section, the high-intensity ultrasonic waves give rise to a pressure dropping under the liquid vapor pressure (2.3 kPa at 20 °C for water) resulting in the generation of fine bubbles in the liquid. During a high-pressure section, the bubbles subsequently explode and release the substantial energy inside. This explosive process gives rise to extraordinary physical and chemical conditions, including high temperature and pressure, strong acoustic streaming, high shear stress, formation of micro-jet, high thermal transfer rate, and the generation of highly reactive hydroxyl radicals (Sutkar and Gogate, 2009). Acoustic cavitation can promote a broad range of physical and chemical reactions and break down various organic compounds in water. The high power input (high cost) and scale-up constraints, however, make the industrial application difficult (Wang et al., 2011a).

### **2.2.2 Hydrodynamic Cavitation**

Hydrodynamic cavitation (HC) is a novel technology that utilizes hydrodynamic energy. It creates the same phenomenon as acoustic cavitation and has the advantages of chemical-free, energy efficiency, and easy scale-up (Gore et al., 2014). This feature may provide a low-cost, eco-friendly technology in the regions where a hydraulic head is available naturally (e.g., communities at high elevations). The easy scale-up property promises its potential to be applied on a large scale (Shah et al., 1999).

Cavitation can occur at the constriction point of a flow-through system. Cavitation bubbles can be found by a sudden pressure change resulting from variation of the liquid velocity in a dynamic flow. Venturi tubes and orifice plates are the most common HC devices because these devices can be manufactured easy and cheaply (Bagal and Gogate, 2014).

#### ***a. Orifice Plate***

Due to its easiness for modification and manufacturability, a number of studies have been conducted using an orifice plate with single or multiple passages (holes) in recent years (Sivakumar and Pandit, 2002; Wu et al., 2011; Braeutigam et al., 2009; Wu et al., 2007; Patil and Gogate, 2012; Wu et al., 2012). To optimize their capacity to generate cavitation, several factors have been investigated including the geometry of the orifice, inlet pressure, fluid temperature, and the concentration of the target contaminants. In a study of the effect of geometry using the multiple-hole orifice plates, Sivakumar and Pandit (2002) found that the extent of rhodamine B degradation increased with: *i*) increasing the ratio of total perimeter of the holes to the total area of the opening ( $\alpha$ ); and

ii) decreasing the ratio of the total flow area (i.e., total area of the holes) to the cross-sectional area of the pipe ( $\beta_o$ ), with a few exceptions. The  $\alpha$  and  $\beta_o$  were calculated using the following formula, respectively,

$$\alpha = \frac{\text{Total perimeter of the holes}}{\text{Total area of opening}} = \frac{n \times 2\pi (d_h/2)}{n \times \pi(d_h/2)^2} = \frac{4}{d_h} \quad (\text{Eq. 2 - 1})$$

$$\beta_o = \frac{\text{Total area of holes}}{\text{The cross section area of the pipe}} = \frac{n \times \pi(d_h/2)^2}{\pi(D/2)^2} = \frac{n d_h^2}{D^2} \quad (\text{Eq. 2 - 2})$$

where  $d_h$  is the diameter of the hole opening (m),  $n$  is the number of holes, and  $D$  is the diameter of the pipe (m). Their results also showed that the extent of the rhodamine B degradation decreased with the increase of the value of the modified cavitation number  $C_v'$ ,

$$C_v' = \frac{C_v}{(\text{Total perimeter of the holes/perimeter of the pipe})} \quad (\text{Eq. 2 - 3})$$

with

$$C_v = \frac{p_2 - p_v}{(1/2)\rho v_o^2} \quad (\text{Eq. 2 - 4})$$

where  $C_v$  is the cavitation number (unit less),  $p_2$  is the fully recovered downstream pressure ( $\text{N/m}^2$ ; Pa),  $p_v$  is the vapor pressure of the liquid ( $\text{N/m}^2$ ; Pa),  $\rho$  is the density of the liquid ( $\text{kg/m}^3$ ), and  $v_o$  is the liquid velocity at the orifice (m/s).

The inlet pressure (upstream pressure or pressure change) is an essential factor that affects the efficiency of HC devices. In a study of degradation of BTEX (benzene, toluene, ethylbenzene, and xylenes), Braeutigam et al. (2009) reported that an optimal inlet pressure was 25 psi (0.17 MPa) based on conversion percentage of toluene in the operating range from 20 to 40 psi (0.14 to 0.28 MPa). The further increase of the inlet pressure from 25 psi resulted in a decrease of the toluene conversion. In the study of the

degradation of methyl parathion, Patil and Gogate (2012) reported that 4 bar (0.40 MPa) is an optimal pressure, as the extent of degradation increased with the increase of the inlet pressure to 4 bar (0.40 MPa) and a further increase in the inlet pressure led to a decrease in the degradation rate.

Temperature is another factor that has been intensively studied. In general, increasing temperature increases the rate of chemical reaction. Also, increasing liquid temperature increases vapor pressure of the liquid, thus it affects the formation of cavities (Wu et al., 2012). A study using phenol as a target compound, Wu et al. (2011) found that an optimal temperature of 20°C for a specific hydrodynamic cavitation setup with a temperature ranges from 16 to 30°C. The degradation rate constant for phenol increased with an increasing temperature up to 20°C. A further increase in temperature decreased the degradation rate. The similar trend was observed in a cavitation study by Wu et al. (2012) with blue-green algae in water: The maximum algal removal percentage was obtained at 20°C. An optimal temperature for the degradation of alachlor by HC was 40°C (Wang and Zhang, 2009).

An initial concentration of a target compound can be an important factor in chemical degradations by HC. In a HC study by Braeutigam et al. (2009), the degradation rate of toluence decreased with increasing its initial concentration. Similar results were reported by Patil and Gogate (2012). In their experiments with four different initial concentrations (20, 30, 40, 50 ppm) of methyl parathion, the highest degradation percentage was obtained from the experiment with the lowest initial concentration (i.e., 20 ppm).

### ***b. Venturi Tube***

A Venturi tube is commonly used as a flow meter in hydraulic engineering systems. Because of its structure and effect, engineers have been exploring its capability as a cavitation device in recent years. The major factors that affect the Venturi cavitator are operating temperature, inlet pressure, and solution pH.

Several studies with a Venturi tube have shown that there is an optimal pressure for cavitation to occur. An increasing inlet pressure can increase the extent of degradation of compounds until it reached the optimal pressure. In a study of the degradation of rhodamine B using a Venturi tube, Mishra and Gogate (2010) reported that, in a range from 2.9 to 5.8 atm (0.29 to 0.59 MPa), the optimal inlet pressure was 4.84 atm (0.45 MPa). The Venturi tube exhibited the similar capability as orifice plate in their study to determine the effect of inlet pressure on the degradation of rhodamine B.

The effect of pH on the degradation of dyes has been studied by several investigators. Aqueous rhodamine B was favorably degraded under the acidic conditions (Mishra and Gogate, 2010). In a study with reactive orange 4 dye, Gore et al. (2014) found that an optimal pH was 3.2 with an optimal inlet pressure of 5 bar (0.50 MPa). In the pH range between 2 and 3.2, the degradation rate increased with increasing pH, and decreased at pH higher than 3.2, confirming the importance of the effect of pH on the degradation of rhodamine B dye in an HC system.

### ***c. Other Cavitation Methods***

In addition to a Venturi tube and an orifice plate, other types of devices such as jets and nozzles have also been studied (Agarwal et al., 2011; Wang et al., 2008; Wang et al., 2009; Wang and Zhang, 2009; Wang et al., 2011a).

#### ***Swirling jet:***

Wang et al. (2008) designed a swirling jet device to create cavitation and studied the effects of the fluid pressure, temperature, and initial concentration, on the degradation of rhodamine B. Varying fluid pressure from 0.2 to 0.6 MPa, they found that the degradation rate of rhodamine B was larger with higher fluid pressure: The largest degradation rate was obtained at 0.6 MPa (87.02 psi).

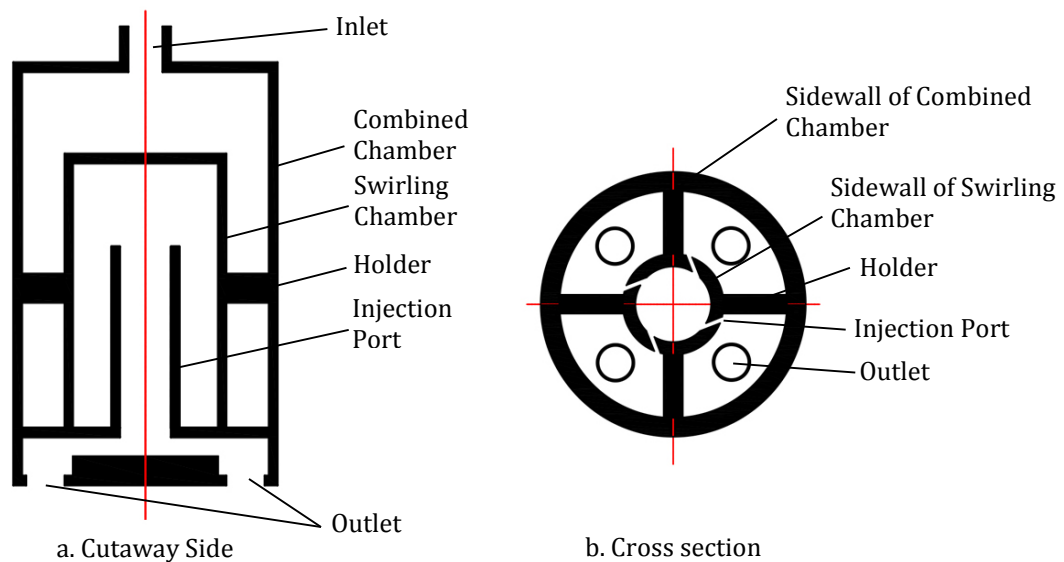


Fig. 2-1 Sketch of combined chamber and swirling cavitation chamber (Wang, et al., 2008)

Wang et al. (2008) also studied the effect of temperature on the degradation of rhodamine B. In the range between 20°C and 60, the optimal temperature was 40 °C. As

was the results of the studies with an orifice and a Venturi tube, the increasing initial concentration led to a decrease of the degradation rate. Similar results were reported by several researchers (Wang and Zhang, 2008; Wang et al., 2009), In their study of swirling jet-induced cavitation to degrade alachlor and K-2BP, they found that the highest degradation of alachlor and K-2BP occurred at 0.6 MPa, 40°C, and 10 mg/L (the lowest initial concentration they studied).

#### ***Combination of HC With Other Methods:***

To improve cost-effectiveness of the cavitation treatment, the hydrodynamic cavitation treatment combined with other methods have been investigated by several researchers. In a study using an orifice plate as a cavitation device and carbamazepine as a target compound, Braeutigam et al. (2012) studied the effect of hydrodynamic cavitation (HC) combined with acoustic cavitation (AC). In their study, under the optimized conditions, the reduction of carbamazepine was over 96% within 15 min. Compared to the sum of individual methods, the synergy of the combined method was calculated to be 63%, indicating a strong synergistic effect between HC and AC.

Using a Venturi tube as a cavitator, Mishra and Gogate (2010) studied the HC method with addition of oxidizing chemicals. In their study, the extent of the degradation of rhodamine B was increased from 59.3% without H<sub>2</sub>O<sub>2</sub> to 99.9% with 200 mg/L of H<sub>2</sub>O<sub>2</sub>. The extent of degradation reached 99.9% after 30 min with Fenton reagent (FeSO<sub>4</sub> : H<sub>2</sub>O<sub>2</sub> = 1 : 5) at the initial rhodamine B concentration of 10 ppm.

## Chapter 3: Experimental

### 3.1 Materials

Reagent grade rhodamine B with a maximum of 0.2% ash (AMRESCO LLC, OH) was used as received. The structural formula of rhodamine B is shown in Fig. 3-1. The molecular formula of rhodamine B is  $C_{28}H_{31}ClN_2O_3$  with molecule weight of 479.02 g/mol.

Rhodamine B solutions were prepared with two different concentrations:  $5.76 \times 10^{-3}$  g/L ( $1.20 \times 10^{-2}$  mM) and  $1.20 \times 10^{-3}$  g/L ( $2.51 \times 10^{-3}$  mM). To prepare the higher concentration solution, 0.80 g/L of a stock solution was prepared by dissolving 0.20 g of powdery rhodamine B in 250 mL of deionized water (DI water). Then 18 mL of the stock solution was diluted into 2.50 L of experiment solution with DI water. This gives  $1.20 \times 10^{-2}$  mM of rhodamine B solution. To prepare the lower concentration solution, 0.10 g of rhodamine B was dissolved in 100 mL of DI water, which gives 1.00 g/L of a stock solution. Then 3 mL of the stock solution was diluted into 2.50 L of experiment solution with DI water. This solution contains  $2.51 \times 10^{-3}$  mM of rhodamine B dye. Deionized water (conductivity) was used for all solution preparation.

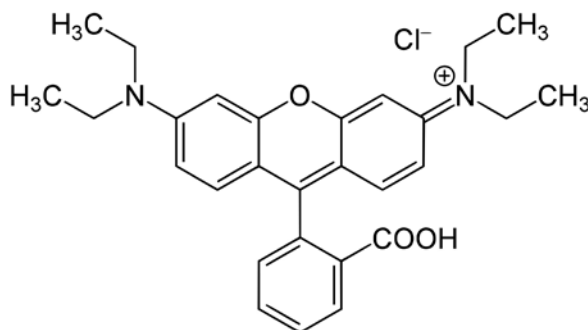


Fig. 3-1 Structural formula of rhodamine B (Yikrazuul, 2008; Jain, et al., 2007)

## 3.2 Experimental Setup

### 3.2.1 HC System Setup

A schematic representation of the pilot-scale water treatment system (continuous recirculating flow system) is shown in Fig. 3-2. A photograph of the system is shown in Fig. 3-3. The treatment system consists of two loops: the inner and outer loops. The inner loop has a tank (Tank 1; 4 in. × 2 ft. Plastic ABS Pipe, VPC Model 1024), a diaphragm pump (SHURflo Model 8030-863-299, 60 Hz, 115 V, 138 W, Costa Mesa, CA), a heat exchanger, and a pressure relief valve (Hypro 3300-0016, New Brighton, MN). The outer loop is comprised of another tank (Tank 2; 4 in. × 2 ft. Plastic ABS Pipe, VPC Model 1024), a pump, a heat exchanger, a pressure relief valve, and a cavitation device. The loop can be switched from the inner loop to the outer loop (or vice versa) using a three-way valve (Valve 2; Dixon BBV100TW). The heat exchanger is connected to a chiller (Neslab CFT-33), which allows the treatment system to maintain a constant temperature. A pressure gauge (Watts Model DPIWTG, North Andover, MA) is located between the cavitation device and the three-way valve (Valve 2). Inlet pressure of the cavitation device can be adjusted using the pressure relief valve located between the pressure gauge and the heat exchanger. The diaphragm pump was used to drive the HC system throughout the experiments.

The cavitation devices tested include Venturi tubes (Mazzei Injector Company, LLC, Bakersfield, CA), orifice plates, and needle tubes. The schematic of various cavitation devices used in this study and their specifications are shown in Fig. 3-4 and Table 2-1, respectively. The Venturi tubes were purchased from Mazzei Injector Company, LLC, Bakersfield, CA. The single- and multiple-hole orifice plates were

constructed using a US dime. Various types of the needle tubes were manufactured by inserting a needle into an orifice's hole. The needles were obtained from Cadence, Inc., Staunton, VA.

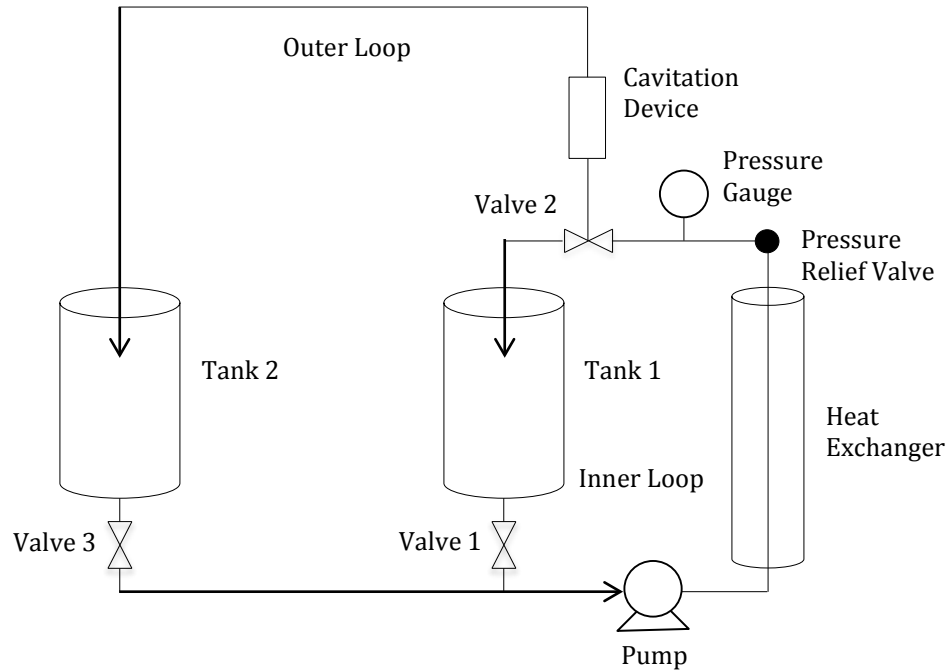
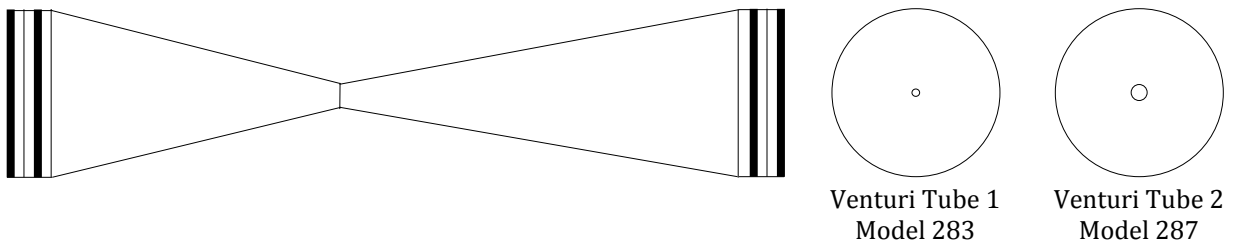


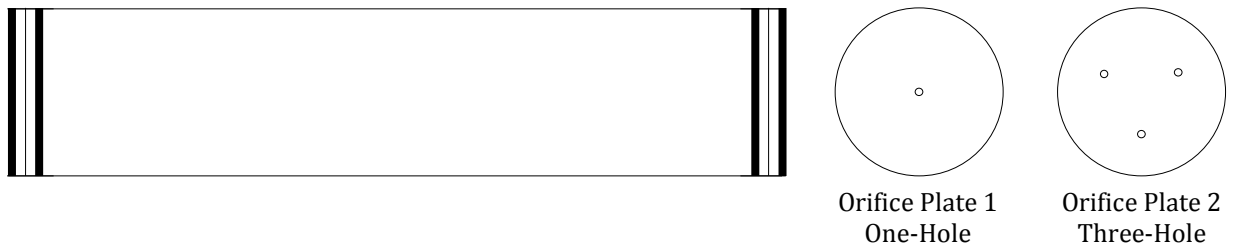
Fig. 3-2 Schematic representation of the hydrodynamic cavitation system



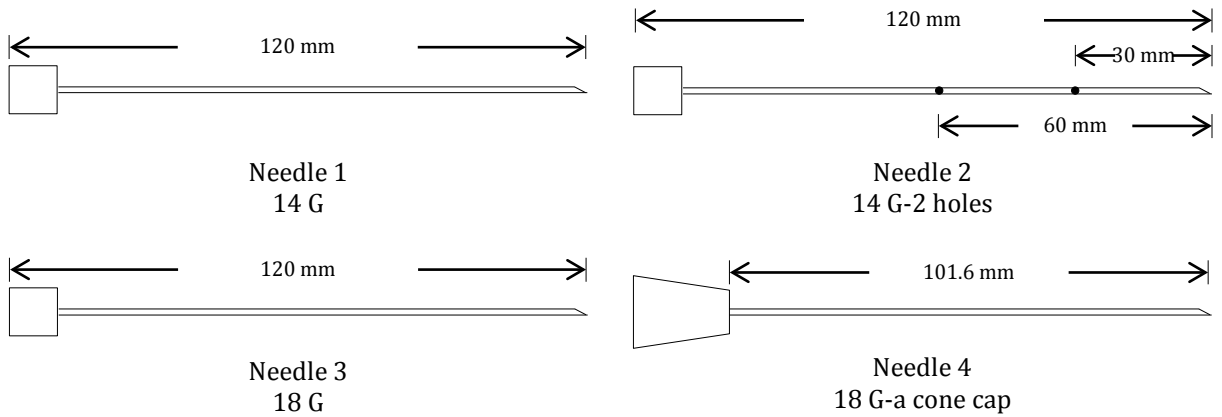
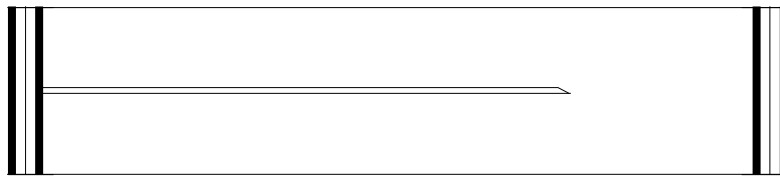
Fig. 3-3 Hydrodynamic cavitation system (Shot by senior design team-Alalkam, Hayes, Howard, Smith)



a. Venturi tubes



b. Orifice plates



c. Needles tubes

Fig. 3-4 The schematic cavitation devices

Table 2-1 Cavitation device information

Device	Constriction point diameter, mm			Comments
Venturi tube #1 (Model 283)	1.6			Estimated
Venturi tube #2 (Model 287)	2			
Orifice Plate #1 (One-hole)	1.32			
Orifice Plate #2 (Three-hole)	1.32			
	Inner, mm	Outer, mm		Wikipedia, 2015; Sigma Aldrich, 2012; Medical Tube Technology, Inc, 2013
		Needle gauge chart	Measured with digital caliper	
Needle Tube #1 (14 G)	1.600 ( $\pm 0.076$ )	2.108 ( $\pm 0.025$ )	2.15	
Needle Tube #2 (14 G/2 holes)				
Needle Tube #3 (18 G)	0.838 ( $\pm 0.038$ )	1.270 ( $\pm 0.013$ )	1.31	
Needle Tube #3 (18 G/1 needle with cone cap)				

### 3.2.2 AC System Setup

A schematic representation of the bench-scale flow-through acoustic cavitation (AC) system is shown in Fig. 3-5. The reactor was modified from the design by previous researchers (Yao, 2006; Nicolae, 2009; Wilson, 2011). The AC system consists of a solution tank, a peristaltic pump (Easy-Load Masterflex Model 7553-70, 6-600 rpm, 75W, Cole-Parmer Instrument Company, Niles, IL) used for feeding solution, and a cylindrical chamber equipped with a US horn (Ultrasonic Processor XL, 50-60 Hz, 110 Volts, 550 W, Misonix Inc., Farmingdale, NY). The US chamber has a diameter of 16 cm, a height of 8.3 cm, and a measured volume of 1.67 L (Wilson, 2011). The ultrasonic power delivered into the aqueous solution was 70% of its rated power.

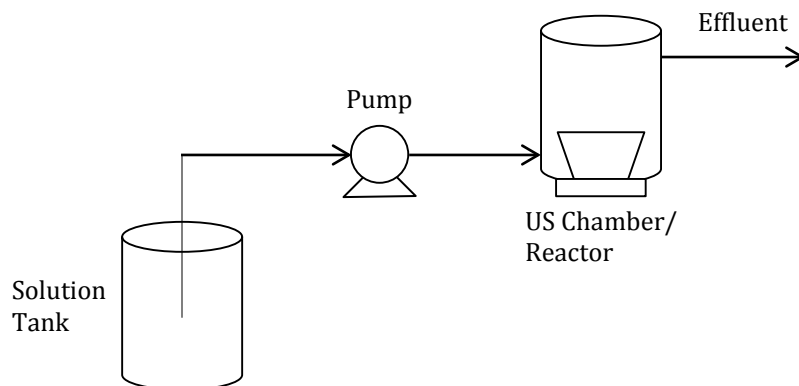


Fig. 3-5 Schematic representation of the acoustic cavitation system

### 3.3 Experimental Procedures

#### 3.3.1 HC System

Each experiment was carried out in two stages, the initial and cavitation stages. The initial stage assures that the test solution is in equilibrium in the treatment system; i.e., uniform dye concentration, constant solution temperature, and absence of bulk of air in the inner loop. To achieve the equilibrium conditions, first, 2.5 L of rhodamine B solution was placed in Tank 1; then the solution was recirculated through inner loop for 20 min. During this stage, the solution was well mixed, temperature was maintained at 20 °C, and air was removed. In this stage, Valve 1 was opened, Valve 3 was closed, and Valve 2 was opened for Tank 1 but closed for Tank 2.

In the cavitation stage, the dye solution was transferred to Tank 2 by opening Valve 2 for Tank 2 (closing for Tank 1). When entire volume of the solution was transferred to Tank 2, Valve 1 was closed; then Valve 3 was opened. As soon as the inlet pressure was adjusted to the target pressure using the pressure relief valve, the initial water sample was collected from the Tank 2 inlet tube. The remaining samples were collected at a 10 min time interval. Each experimental run lasted for 100 min.

In addition to the types of cavitation devices, the effect of inlet pressure ranging from 30 to 70 psi (0.207 MPa to 0.483 MPa) was examined. The effect of the initial concentration of rhodamine B dye was also studied at  $1.20 \times 10^{-2}$  mM and  $2.51 \times 10^{-3}$  mM.

### **3.3.2 AC System**

The operating procedures of AC system were modified from the design by Wilson (2011). 20 liters of rhodamine B solution with a concentration of  $1.20 \times 10^{-2}$  mM was prepared for each experimental run. The flow rate was 100 mL/min. The water samples were taken from the effluent of the reactor at an 8 min interval during the first 72 min. The remaining 2 samples were collected at a 14 min and 20 min intervals respectively. Each run lasted for 106 min.

### **3.4 Analysis**

A water sample was analyzed for the concentration of dye and pH immediately after the sample was collected. The concentration of rhodamine B dye was analyzed with UV-vis spectrophotometer (Hewlett Packard 8452A Diode Array Spectrophotometer, Agilent Technologies, Inc., Santa Clara, CA) at 554 nm wavelength (Sivakumar and Pandit, 2001; 2002.). pH of the solution was measured by a pH meter (Thermo Scientific Orion™ Star A121). Temperature of the solution was measured in Tank 1 (in the initial stage) and Tank 2 (in the cavitation stage) with a thermometer (15-077-8D, Fisher Scientific™ Traceable™, Pittsburgh, PA).

## Chapter 4: Results and Discussion

### 4.1 Preliminary Study

A preliminary study was conducted to select effective cavitation devices. Cavitation devices were examined visually by observing an extent of generation of micro- and nano-bubbles and by determining the percent degradation of rhodamine B. Experiments were carried out at the initial dye concentrations of  $2.51 \times 10^{-3}$  mM (except for Venturi tube #2: Model 287) and  $1.20 \times 10^{-2}$  mM. Results were summarized in Table 4-1. It is noteworthy that fine bubbles were produced only by the Venturi tubes (Model 283 and 287), and that the concentration of rhodamine B dye reduced more by the Venturi tubes than other devices. The poor performance by the orifice plates and needle tubes can be attributed to unbalance between the sizes of openings, pressure, and flow velocity. Due to the process design constraints, there was limited control of inlet pressures of the orifice plates and needle tubes: We could not reduce the inlet pressure below 60 psi (0.414 MPa) for the orifice and 70 psi (0.483 MPa) for the needle tubes. The orifice plates and needle tubes failed to generate micro-bubbles. The failure can be explained as follows. Under a high fluid pressure, flowing fluid would bounce back from the wall of the orifice plate (or needle tube) resulting in an inefficient energy use. This might be a reason for poor performance of the orifice plates and needle tubes. A gradual reduction of opening (passage way) may be required for generation of hydrodynamic cavitation. The geometry of cavitation device is likely one of the major design parameters that affect the efficiency and initiation of cavitation in an aqueous solution. More studies are required to examine the effect of geometry of various cavitation devices on their

efficiency. In future study, we suggest that a bypass line be placed between the feed pump and the cavitation device, which provides us more operational flexibility when lowering inlet pressure is required.

Table 4-1 Preliminary study of cavitation devices

Cavitation Device	Generation of nano- or micro-bubbles	Degradation of rhodamine B, $C_n/C_o$ <sup>c</sup>	Comments
Venturi Tube #1 (Model 283)	Yes <sup>a</sup>	3.94% ( $P_{in} = 50$ psi); 10.6% ( $P_{in} = 60$ psi); 16.4% ( $P_{in} = 70$ psi).	Inlet pressure could not reach over 76 psi (a fluctuation shown on the pressure gauge)
Venturi Tube #2 (Model 287)	Yes <sup>a</sup>	8.75 % ( $P_{in} = 50$ psi)	Inlet pressure could not reach over 55 psi (a fluctuation shown on the pressure gauge) – probably due to larger throat diameter
Orifice Plate #1 (One-hole)	No <sup>b</sup>	1.32% ( $P_{in} = 60$ psi); 2.00% ( $P_{in} = 100$ psi).	Inlet pressure could not reach under 60 psi – probably due to the small diameter of the hole
Orifice Plate #2 (Three-hole)	No <sup>b</sup>	N/A <sup>d</sup>	N/A <sup>d</sup>
Needle Tube #1 (14 G)	No <sup>b</sup>	N/A <sup>d</sup>	Inlet pressure could not reach under 70 psi – probably due to the small diameter of the hole
Needle Tube #2 (14 G-2 holes)	No <sup>b</sup>	N/A <sup>d</sup>	Inlet pressure could not reach under 70 psi – probably due to the small diameter of the hole
Needle Tube #3 (18 G)	No <sup>b</sup>	N/A <sup>d</sup>	Inlet pressure could not reach under 70 psi – probably due to the small diameter of the hole
Needle Tube #4 (18 G-a cone cap)	No <sup>b</sup>	N/A <sup>d</sup>	Inlet pressure could not reach under 70 psi – probably due to the small diameter of the hole

a. Numerous of fine bubbles were observed throughout experiments;

b. Many tiny bubbles were observed at the beginning of the experiment. After the entire cavitation tube was filled with the test solution, no bubbles were observed. The fine bubbles found in the beginning of the run can be attributed to air present in the pipes of the system;

c. The extent of degradation of rhodamine B,  $C_n/C_o$ , was defined as the following equation:

$$C_n/C_o = \frac{C_o - C_t}{C_o} \%$$

where  $C_t$  = concentration of rhodamine B at time t min (mM),  $C_o$  = initial concentration of rhodamine B (mM), and  $C_n$  = concentration difference between  $C_t$  and  $C_o$  (mM).

d. Experimental data not available. Since no bubbles were observed for orifice plates and needle tubes (no hydrodynamic cavitation happened), no further experiments were conducted;

e.  $P_{in}$  = inlet pressure.

## 4.2 Degradation Kinetics

The degradation kinetics of rhodamine B was investigated for two different models of Venturi tubes (Model 287 and Model 283). In studies by other investigators, an optimal inlet pressure was found to be around 70 psi (0.483 MPa) (Wang et al., 2008; Mishra and Gogate, 2010; Patil and Gogate, 2012; Gore et al., 2014;). In this study, cavitation was induced by the Venturi Tube #1 (Model 283) at the inlet pressure of 70 psi and initial dye concentration of  $1.20 \times 10^{-2}$  mM. In order to determine the reaction order, the normalized dye concentrations ( $C_t/C_0$ ) are plotted in (a) with a linear-regression line and (b) with an exponential trendline in Fig. 4-1. As is seen, both plots exhibited the coefficient of determination ( $R^2$ ) value of 0.966, indicating that the reaction order can be either the zero<sup>th</sup>-order or first-order, with the rate constants of  $6.23 \times 10^{-6}$  mM/min or  $5.31 \times 10^{-4}$  min<sup>-1</sup>, respectively.

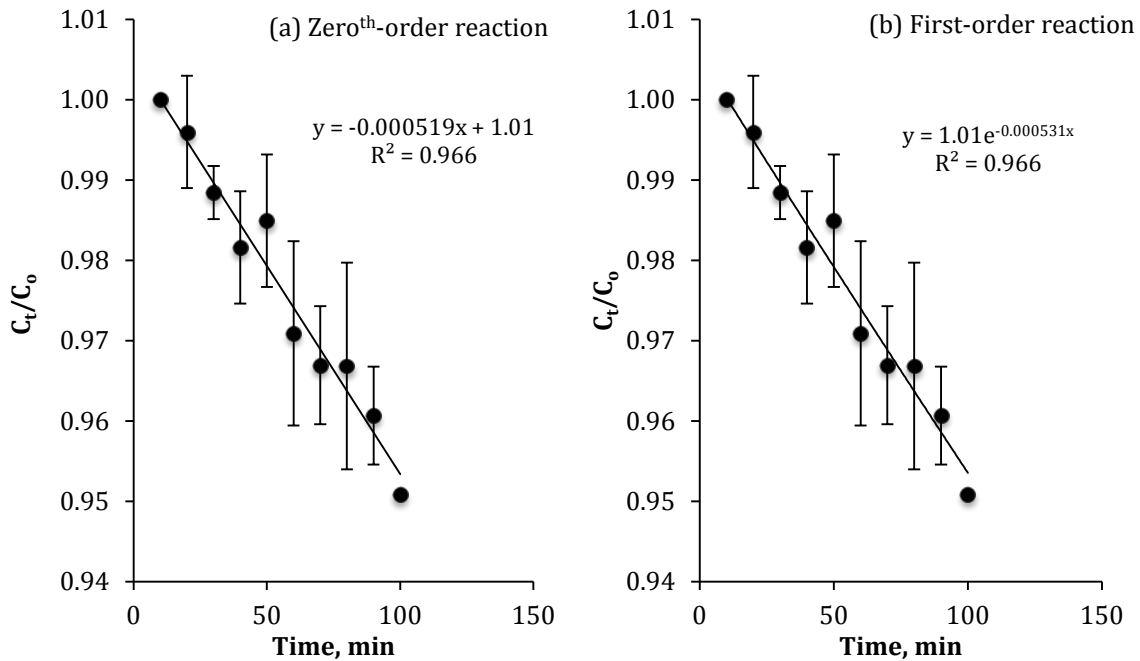


Fig. 4-1 Degradation of rhodamine B with Venturi tube #1 (Model 283) with inlet pressure of 70 psi (0.483 MPa) and initial dye concentration of  $1.20 \times 10^{-2}$  mM: (a) zero<sup>th</sup>-order kinetics; (b) first-order kinetics.

For the Venturi tube #2 (Model 287), we could not increase the inlet pressure over 55 psi (0.379 MPa) probably due to the larger throat size (ca. 2 mm). Accordingly, experiments with the Venturi tube #2 (Model 287) were conducted at the inlet pressure of 50 psi (0.345 MPa) with the initial dye concentration of  $1.20 \times 10^{-2}$  mM. As was the Venturi Tube #1 (Model 283), the normalized dye concentrations ( $C_t/C_0$ ) are presented in (a) with a linear-regression line and (b) with an exponential trendline in Fig. 4-2. The results show that the dye degradation reaction follows either the zero<sup>th</sup>-order or first-order kinetics with the degradation rate constant of  $1.24 \times 10^{-5}$  mM/min ( $R^2 = 0.977$ ) or  $1.09 \times 10^{-3} \text{ min}^{-1}$  ( $R^2 = 0.978$ ), respectively.

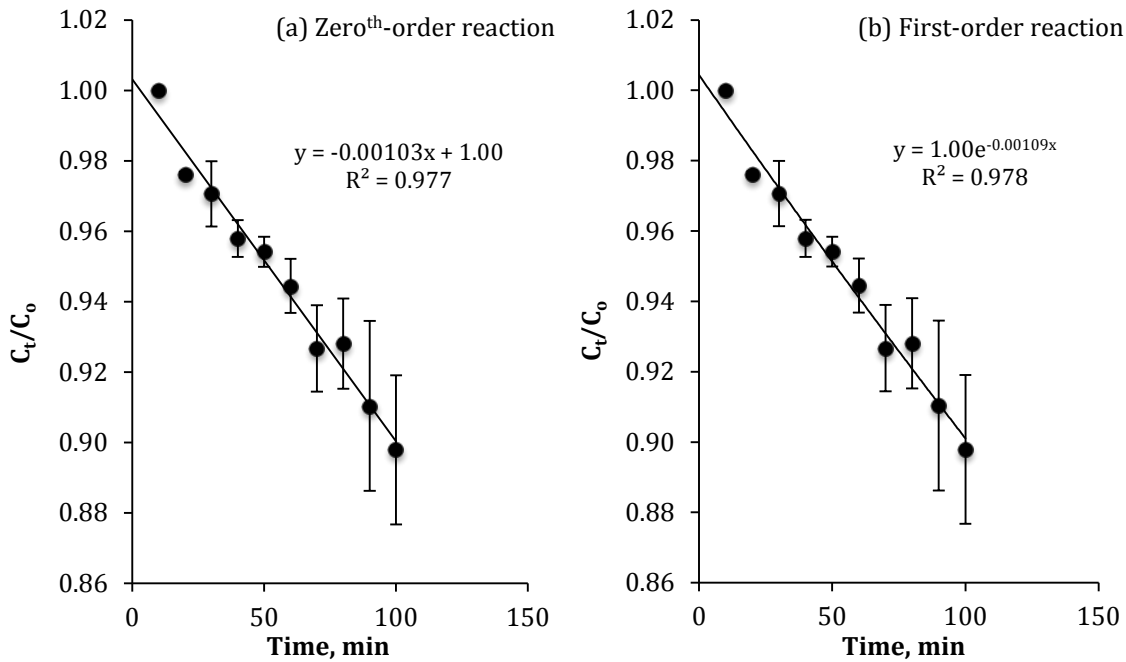


Fig. 4-2 Degradation of rhodamine B with the Venturi tube #2 (Model 287) with inlet pressure of 50 psi (0.344 MPa) and initial dye concentration of  $1.20 \times 10^{-2}$  mM: (a) zero<sup>th</sup>-order kinetics; (b) first-order kinetics.

According to the results presented in Figs. 4-1 and 4-2, the degradation of rhodamine B can be expressed by either zero<sup>th</sup>- or first-order kinetics. The reaction kinetics results reported by this and other researchers are summarized in Table 4-2.

Sivakumar and Pandit (2002) expressed the degradation rate of rhodamine B by HC using the first-order reaction kinetics. In a study with the swirling jet-induced cavitation, the degradation of reactive red K-2BP followed the first-order kinetics (Wang et al., 2011a). Gore et al. (2014) expressed the decolorization rate of reactive orange 4 dye by HC using a first-order reaction. In the present study for the degradation of rhodamine B, there is little significant difference between the zero<sup>th</sup>-order and the first-order expression, which can be attributed to small change in dye concentration (small degree of degradation).

Table 4-2 Reaction kinetics with various cavitation devices and compounds

Reaction kinetics	Cavitation device	Compound (degraded)	Conditions	Reference
First-order	Circular Venturi tube	Reactive orange 4 dye	$P_{in} = 3-8$ bar, $C_o = 40$ ppm, pH = 2, T = N/A	Gore et. al. (2014)
First-order	Multi-holes orifice plate	Rhodamine B	$P_{in} = 30$ psi, $C_o = 5-6$ $\mu$ g/mL, T = 35-40 °C	Sivakumar and Pandit (2002)
First-order	Swirling jet	K-2BP	$P_{in} = 0.6$ MPa, $C_o = 20$ mg/L, pH = 5.5, T = 323 K, additive ( $H_2O_2$ , 300 mg/L)	Wang et al. (2011a)
First-order	Venturi tube #1 (Model 283)	Rhodamine B	$P_{in} = 70$ psi, $C_o = 1.20 \times 10^{-2}$ mM, T = 20 °C	This work
First-order	Venturi tube #2 (Model 287)	Rhodamine B	$P_{in} = 50$ psi, $C_o = 1.20 \times 10^{-2}$ mM, T = 20 °C	This work

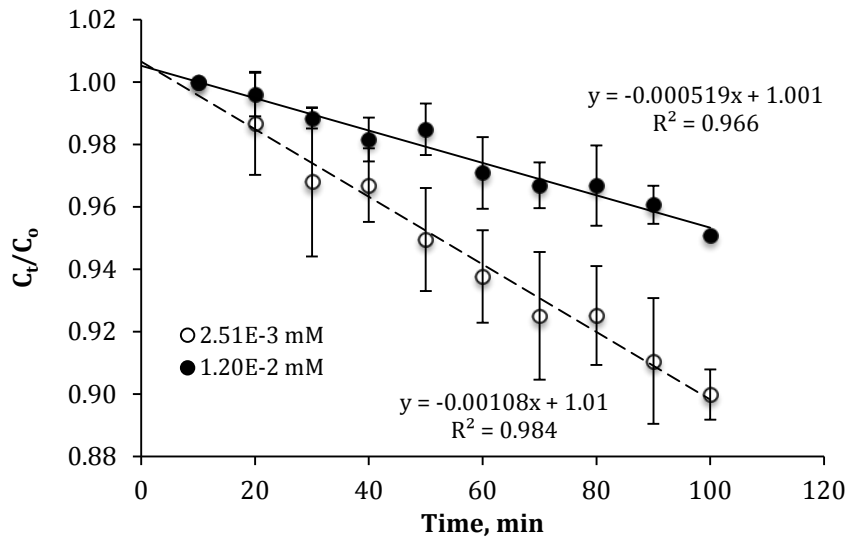
\*  $P_{in}$ , inlet pressure;  $C_o$ , initial concentration of compound; T, solution temperature.

### 4.3 Effect of Dye Concentration

Fig. 4-3 shows the degradation of rhodamine B with the Venturi tube #1 (Model 283) at an inlet pressure of 70 psi (0.482 MPa) and two different initial concentrations:  $1.20 \times 10^{-2}$  and  $2.51 \times 10^{-3}$  mM. The degradation rate constants of rhodamine B are  $2.71 \times 10^{-6}$  mM/min (zero<sup>th</sup>-order) and  $1.14 \times 10^{-3}$  min<sup>-1</sup> (first-order) at  $2.51 \times 10^{-3}$  mM, and  $6.23 \times 10^{-6}$  mM/min (zero<sup>th</sup>-order) and  $5.31 \times 10^{-4}$  min<sup>-1</sup> (first-order) at  $1.20 \times 10^{-2}$  mM.

Theoretically, the rate constant is independent of the reactant concentration in the zero<sup>th</sup>-order reaction. Because our results showed that the rate constant varied with the initial concentration of the dye, the possibility of zero<sup>th</sup>-order reaction is eliminated, and, hereafter, the degradation of rhodamine B by HC is expressed using the first-order kinetics.

a) Zero<sup>th</sup>-order



b) First-order

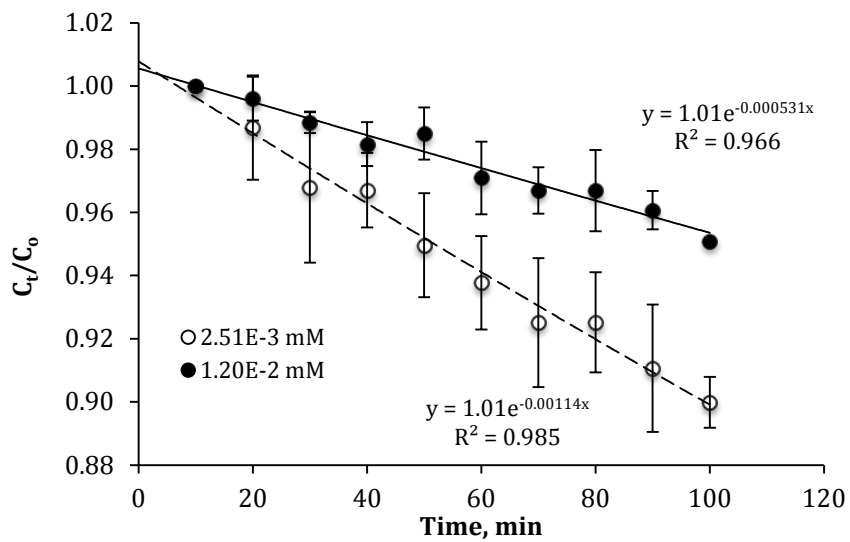
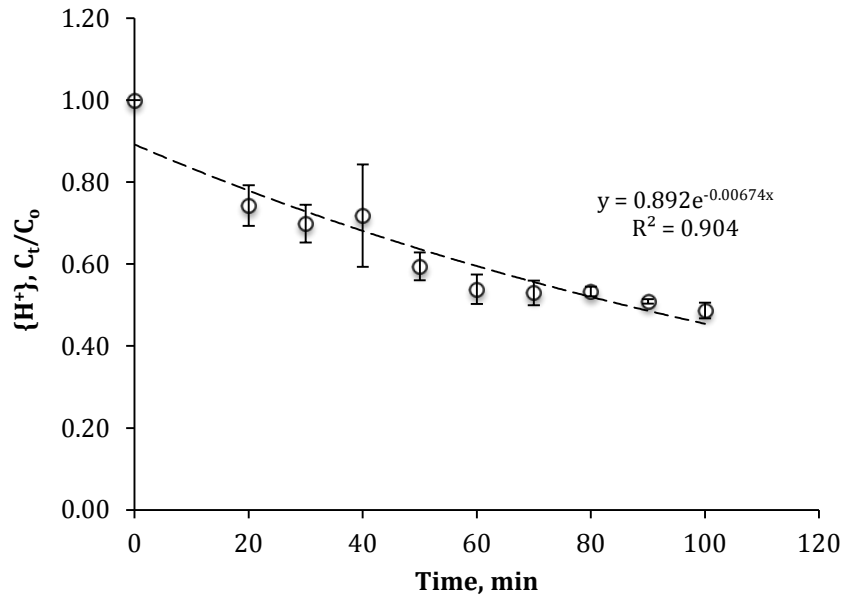


Fig. 4-3 First order degradation of rhodamine B with Venturi tube #1 (Model 283) with inlet pressure of 70 psi (0.483 MPa) and two different initial concentrations of dye:  $1.20 \times 10^{-2}$  mM and  $2.51 \times 10^{-3}$  mM.

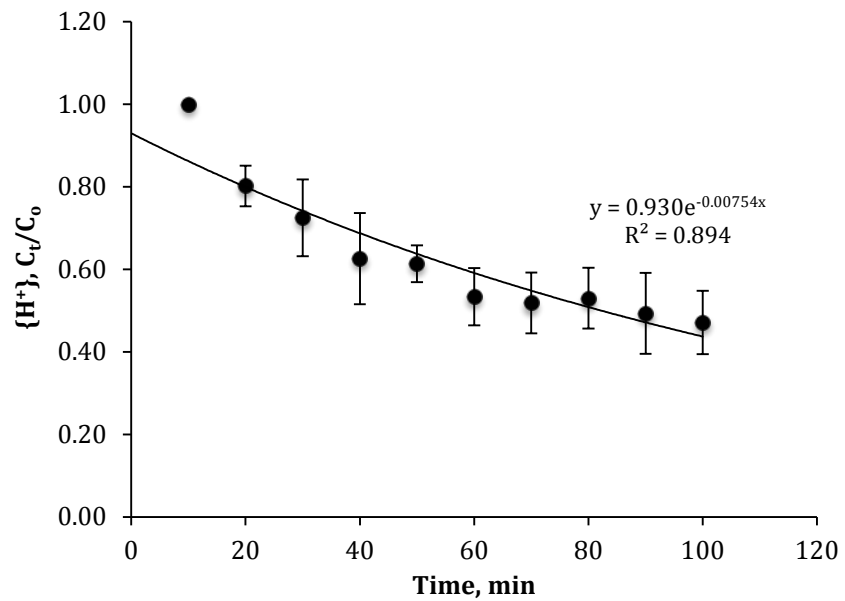
The major mechanism of the degradation of rhodamine B by HC is expected to be oxidation by hydroxyl radicals ( $\bullet\text{OH}$ ). For given conditions (HC device, inlet pressure, temperature, flow rate), the number of hydroxyl radicals produced is constant. At a high dye concentration, the dye removal efficiency,  $E = (C_o - C)/C_o$ , is small because the number of dye molecules in a solution is large. On the other hand, the dye removal efficiency is large at a low dye concentration because the number of dye molecules in a solution is small, resulting in a larger degradation rate constant value. In our study, we observed the lower degradation rate constant at the higher initial concentration, which could be attributed to the competition among the pollutant (dye) molecules for  $\bullet\text{OH}$  (Wang et al., 2011a). In a study with methyl parathion over a concentration range of 20-50 ppm, Patil and Gogate (2012) found that the removal efficiency (44.44%) was highest at the lowest initial concentration (20 ppm). Wang et al. (2011a) also reported the similar result in their study with brilliant red K-2BP in a concentration range of 10-50 mg/L.

#### **4.4 Dye Solution pH**

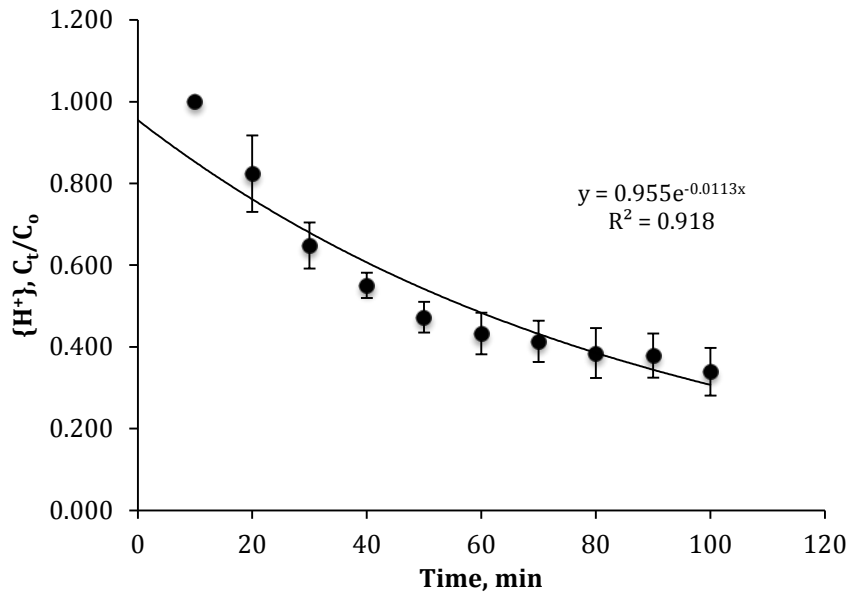
The hydrogen-ion activity of a dye solution during the HC treatment is investigated based on the experimental data obtained with two Venturi tubes (Model 283 and Model 287). The hydrogen-ion activity was measured as pH. The result was shown in Fig. 4-4, Fig. 4-5 and Fig. 4-6. As is seen, the hydrogen-ion activity of the dye solution exponentially decreased with time, indicating that the dye molecules were degraded with an exponential rate. This results also indicate that the reaction is not zero<sup>th</sup>-order.



4-4. Hydrogen-ion activity of dye solution through HC process with Venturi tube #1 (Model 283): inlet pressure 70 psi, initial concentration  $2.51 \times 10^{-3}$  mM ( $\{H^+\} = 10^{-pH}$  mM).



4-5. Hydrogen-ion activity of dye solution through HC process with Venturi tube #1 (Model 283): inlet pressure 70 psi, initial concentration  $1.20 \times 10^{-2}$  mM ( $\{H^+\} = 10^{-pH}$  mM).



4-6. Hydrogen-ion activity of dye solution through HC process with Venturi tube #2 (Model 287): inlet pressure 50 psi, initial concentration  $1.20 \times 10^{-2}$  mM ( $\{H^+\} = 10^{-pH}$  mM).

According to the molecular structure of rhodamine B, one carboxyl group is attached to the benzene ring, which makes the dye solution acidic. The decreasing of hydrogen-ion activity in the dye solution can be attributed to the degradation of a carboxyl group of rhodamine B.

#### 4.5 Comparison of Two Venturi Tubes

The performances of two Venturi tubes (Model 283 and Model 287) are summarized in Table 4-3. The percent removal of rhodamine B was calculated using:

$$\% \text{ Removal} = 1 - \frac{C_t}{C_o} \quad (\text{Eq. 4 - 1})$$

where  $C_o$  = initial concentration of rhodamine B dye, and  $C_t$  = concentration of rhodamine B dye at  $t = 100$  min.  $C_t/C_o$  was obtained from the exponential regression

equation. As is seen, the Venturi tube #2 (Model 287) provide the best overall performance with the largest percent removal, largest flow rate, and lowest inlet pressure. The lower operating fluid pressure means lower operational costs, if a pump is used to create HC.

Table 4-3 Summary of experimental results of Venturi tubes (Model 283 and Model 287)

Cavitation Device	Measured initial dye conc. <sup>a</sup> , mM	Degradation rate constant <sup>b</sup> , k, min <sup>-1</sup>	Flow rate, mL/min	Inlet pressure, psi	% Removal of rhodamine B in 100 min <sup>c</sup>
Venturi tube #1 (Model 283)	$1.45 \times 10^{-3}$	$1.14 \times 10^{-3}$	2626.66	70	9.88 %
Venturi tube #1 (Model 283)	$9.49 \times 10^{-3}$	$5.31 \times 10^{-4}$	2492.56	70	4.22 %
Venturi tube #2 (Model 287)	$8.74 \times 10^{-3}$	$1.09 \times 10^{-3}$	2990.84	50	10.33 %

a. Measured initial concentration of rhodamine B, (mM);

b. Degradation rate constants were evaluated based on first-order reaction;

c. Calculation refers appendix C;

d.  $C_t$  = Concentration of rhodamine B at time t min (mM);  $C_o$  = Initial concentration of rhodamine B (mM).

#### 4.6 Effect of Inlet Pressure

The effect of inlet pressure on the degradation rate of rhodamine B was evaluated using the Venturi tube #2 (Model 287) with an inlet pressure range of 30-55 psi (0.207-0.379 MPa) and the initial dye concentration of  $1.20 \times 10^{-2}$  mM. Results are summarized in Table 4-4 and shown in Fig. 4-5. The result indicates that there is an optimal inlet pressure for the degradation of rhodamine B. The extent of degradation increased with increasing inlet pressure from 30 psi (0.207 MPa) to 50 psi (0.344 MPa). A further increase in the inlet pressure lead to a decrease in the degradation rate, giving an optimal inlet pressure of 50 psi (0.344 MPa).

The increasing degradation rate with increasing inlet pressure can be attributed to increasing hydroxyl radicals. Under the higher inlet pressure, the collapse of micro- or nano-bubbles becomes more violent leading to the generation of higher pressure pulses, which could have enhanced the dissociation of water molecules to  $\cdot\text{OH}$  and  $\cdot\text{H}$  (Gogate and Pandit, 2001). This phenomenon can also be explained by the cavitation number. The cavitation number,  $C_v$ , is defined as (Wu et al., 2007):

$$C_v = \frac{p_d - p_v}{(1/2)\rho v_0^2} \quad (\text{Eq. 4 - 2})$$

or

$$C_v = \frac{p_u - p_v}{p_u - p_d} \quad (\text{Eq. 4 - 3})$$

where  $p_u$ ,  $p_d$ , and  $p_v$  are the upstream pressure, downstream pressure, and fluid's vapor pressure, respectively.  $\rho$  is the density of the fluid and  $v_0$  is the fluid velocity at the throat of the cavitation unit. Generally, an increase of the upstream pressure (inlet pressure) would give raise to an increase of the cavitation number,  $C_v$  and increases the number of cavitation events (Suslick et al., 1997; Wu et al., 2007). In other words, cavitation effects are enhanced under the higher inlet pressure condition up to a certain pressure. The decrease of the dye degradation beyond a certain inlet pressure can be attributed to the condition known as "supercavitation." Under the super cavitation conditions, volumetric concentrated cavities start to coalesce with each other and form vaporous cloud in downstream, leading to a decrease in the formation of hydroxyl radicals (Saharan et al., 2011; Gore et al., 2014).

Results in Table 4-4 showed that the first-order degradation rate constant increased from  $6.59 \times 10^{-4}$  to  $1.11 \times 10^{-3} \text{ min}^{-1}$  when the inlet pressure increased from 30

psi (0.207 MPa) to 50 psi (0.344 MPa). Further increase of the inlet pressure to 55 psi lead to the decrease of the degradation rate constant to  $7.68 \times 10^{-4} \text{ min}^{-1}$ . The maximum degradation rate constant ( $1.11 \times 10^{-4} \text{ min}^{-1}$ ) was observed at the inlet pressure of 50 psi. Patil and Gogate (2012) conducted experiments with a pressure range of 1-8 bar (0.1-0.8 MPa), and observed the maximum extent of the degradation of methyl parathion at 4 bar (0.4 MPa), which is similar to our results. The optimal inlet pressure of 5 bar (0.5 MPa) was reported by Gore et al. (2014) in their study with reactive orange 4 dye.

Our results and others suggest that there is an optimal inlet pressure that gives the largest cavitation effect. The optimal inlet pressure is likely dependent on the design of constriction of the cavitation device. The results also suggest that, for a well-designed cavitation device, desired cavitation events can be produced at a considerably lower fluid pressure. Such a cavitation device can reduce the operation costs and energy consumption (Patil and Gogate, 2012). This also allows an idea of utilizing elevation head (hydraulic head) to produce a high pressure that drives the fluid flows through a cavitation device, generating  $\cdot\text{OH}$ . This HC technology can be used more effectively in communities in high-elevation regions where hydrodynamic energy is readily available: The energy cost for operating the HC device is nil.

Table 4-4 Summary of experiment data for different inlet pressure

Run ID /Date	Measured initial conc. <sup>a</sup> , mM	Inlet pressure, Psi	Temp., °C	Degradation rate constant <sup>b</sup> , k, min <sup>-1</sup>	R <sup>2</sup> <sup>c</sup>	Average, k, min <sup>-1</sup>	STD
8/16/15	$8.76 \times 10^{-3}$	30	20	$6.61 \times 10^{-4}$	0.881	$6.59 \times 10^{-4}$	$4.49 \times 10^{-7}$
8/17/15	$9.26 \times 10^{-3}$	30	20	$7.13 \times 10^{-4}$	0.758		
8/18/15	$9.77 \times 10^{-3}$	30	20	$6.03 \times 10^{-4}$	0.831		
7/31/25	$9.45 \times 10^{-3}$	40	20	$8.20 \times 10^{-4}$	0.882	$9.41 \times 10^{-4}$	$1.29 \times 10^{-6}$
8/3/15	$8.59 \times 10^{-3}$	40	20	$8.82 \times 10^{-4}$	0.927		
8/14/15	$9.27 \times 10^{-3}$	40	20	$1.12 \times 10^{-3}$	0.800		
7/15/15	$8.21 \times 10^{-3}$	50	20	$1.05 \times 10^{-3}$	0.880	$1.11 \times 10^{-3}$	$2.38 \times 10^{-6}$

7/16/15	$8.92 \times 10^{-3}$	50	20	$1.43 \times 10^{-3}$	0.921		
7/28/15	$9.10 \times 10^{-3}$	50	20	$8.57 \times 10^{-4}$	0.921		
8/8/15	$8.80 \times 10^{-3}$	55	20	$6.82 \times 10^{-4}$	0.734	$7.68 \times 10^{-4}$	$2.36 \times 10^{-6}$
8/9/15	$9.05 \times 10^{-3}$	55	20	$5.32 \times 10^{-4}$	0.826		
8/10/15	$1.01 \times 10^{-2}$	55	20	$1.09 \times 10^{-3}$	0.853		

- a. Measured initial concentration of rhodamine B, (mM);  
b. All degradation rate constants were evaluated based on first-order reaction;  
c. R2 were performed with Microsoft Excel for Mac 2011;

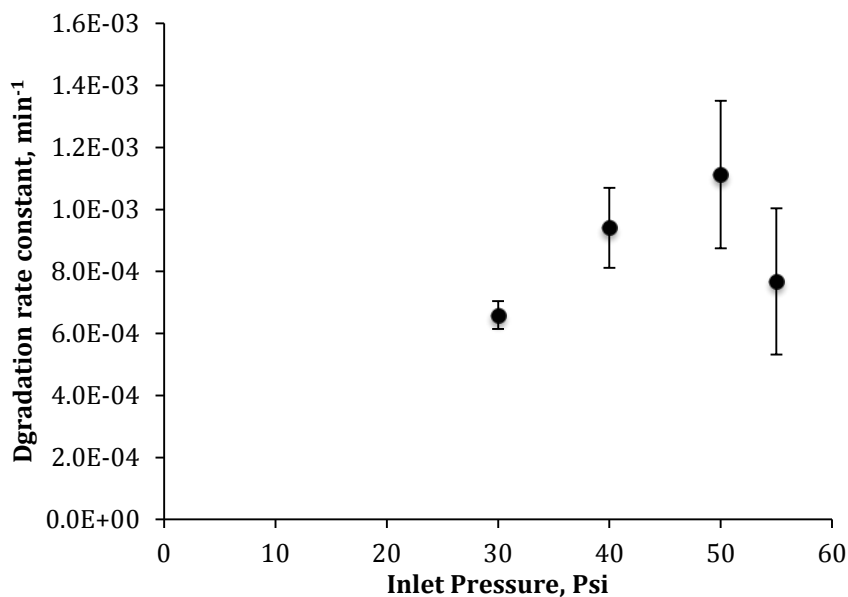


Fig. 4-7 Degradation rate constant of rhodamine B at different inlet pressure: Venturi tube #2 (Model 287), initial concentration  $1.20 \times 10^{-2}$  mM

#### 4.7 Comparison of Energy Efficiency between HC and USUV System

The energy usage by HC system with two Venturi tubes (Model 283 and Model 287) was compared to that by the acoustic cavitation (AC) system. A comparison was made with the cavitation yield, which is defined as the extent of degradation of rhodamine B per unit energy used (mM/J). Results are presented in Table 4-5.

Table 4-5 Summary of HC and US system

Cavitation device	Measured initial conc. <sup>a</sup> , mM	Flow rate, mL/min	Inlet pressure, psi	Temp., °C	Degradation rate constant <sup>b, c</sup> , k, min <sup>-1</sup>	Treated Volume, L	% Removal of rhodamine B in 100 min <sup>c</sup>
Venturi tube #1	$1.45 \times 10^{-3}$	2626.66	70	20	$1.14 \times 10^{-3}$	2.50	9.88 %

(Model 283)							
Venturi tube #1 (Model 283)	$9.49 \times 10^{-3}$	2492.56	70	20	$5.31 \times 10^{-4}$	2.50	4.22 %
Venturi tube #2 (Model 287)	$8.74 \times 10^{-3}$	2990.84	50	20	$1.09 \times 10^{-3}$	2.50	10.33 %
Ultrasound	$1.04 \times 10^{-2}$	100	N/A	15-39	$4.19 \times 10^{-3}$	10	6.534 % (in 16.7 min)

- a. Measured initial concentration (Real concentration) of rhodamine B dyes, mM;  
b. All degradation rates were estimated based on first-order reaction;  
c. Calculation refers to Appendix C.

The energy efficiencies of all processes were compared based on the extent of degradation of rhodamine B in the first 100 min (as the duration of the HC experiment was 100 min). The percent removal of rhodamine B with Venturi tubes were calculated using Eq. 4-2. The result in Table 4-5 shows that the HC system with the Venturi tube #2 exhibited the largest removal efficiency (10.33 %) under a lower inlet pressure among the HC experiments. The degradation rate constant of HC system with the Venturi tube #2 is about one-fourth of the AC system ( $4.19 \times 10^{-3}$  mM/min).

The energy efficiency of HC and AC processes were calculated as follow:

Total mmol of rhodamine B removed in 100 min

= (Dye conc. reduced within 100 min) mmol/L  $\times$  (Treated Volume) L

Energy input to the system in 100 min

= (Power input) Watt  $\times$  (Treatment time) s

Energy efficiency

= (Total rhodamine B removed within 100 min) mmol/(Energy input) J

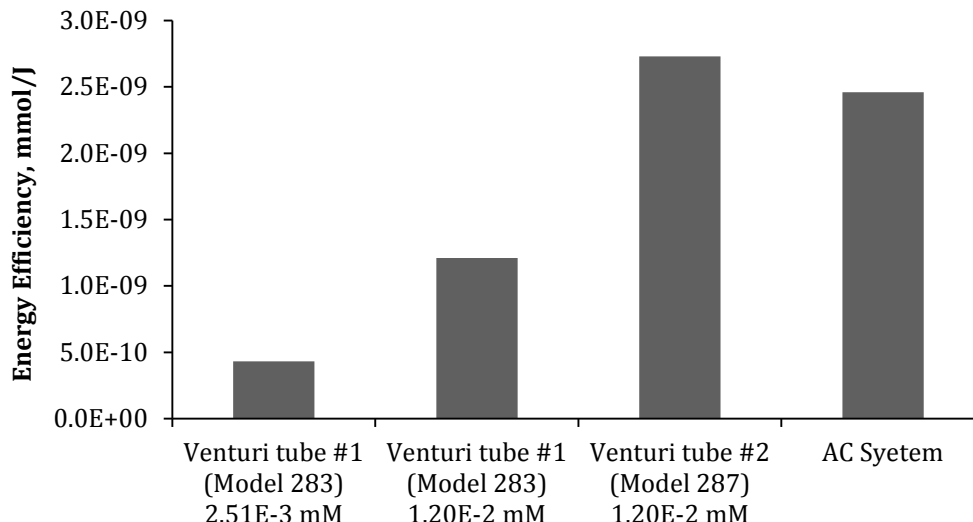


Fig. 4-8 Comparison of Energy Efficiency between HC and USUV System

As is seen in Fig. 4-8, the Venturi tube #2 (Model 287) gave the highest energy efficiency when it was run with the initial concentration of  $1.20 \times 10^{-2}$  mM and the inlet pressure of 50 psi (0.345 MPa). The Venturi tube #2 (Model 287) was 10 % more energy efficient than the AC system. The result suggests that an HC system is a more cost-effective method than the AC system. Obviously, further studies are needed to design more effective cavitation devices and identify optimal conditions for generating hydroxyl radicals.

## Chapter 5: Conclusion

Environmental problems caused by large volume of tainted wastewater attracted our attentions. A pilot-scale hydrodynamic cavitation (HC) system was investigated as a potential application to degrading rhodamine B dye in water. A series of experiments were carried out in a continuously recirculating flow system to evaluate three types of cavitation devices (i.e., orifice plates, Venturi tubes, needle tubes). The degradation kinetics of Rhodamine B dye was examined with the following physical and chemical parameters: *i*) initial concentration of the dye, *ii*) hydrogen-ion activity of the dye solution, and *iii*) inlet pressure of the cavitation devices. Among the devices tested, the Venturi tube #2 (Model 287) showed the best performance with the removal efficiency of 10.33 %, the first-order degradation rate constant of  $1.09 \times 10^{-3} \text{ min}^{-1}$  at the inlet pressure of 50 psi (0.345 MPa) and the initial dye concentrations of  $8.74 \times 10^{-3} \text{ mM}$ . In a comparison of the degradation of the dye by hydrodynamic cavitation with that by acoustic cavitation (AC), the HC system with the Venturi tube #2 (Model 287) was about 10 % more energy efficient than the AC system with the ultrasound sonicator. Further studies are needed to design more effective cavitation devices and identify optimal conditions for generating hydroxyl radicals. Studies on utilization of natural hydraulic head that replaces a water pump are required to develop a sustainable, cost-effective HC water treatment technology in the future.

## References

- Adeyemi, Y.G., 2005. Sonochemistry in environmental remediation. 2. Heterogeneous sonophotocatalytic oxidation processes for the treatment of pollutants in water. *Environmental Science and Technology*, 39: 8557-8570.
- Agarwal, A., Ng, W. J. and Liu, Y., 2011. Principle and applications of microbubble and nanobubble technology for water treatment. *Chemosphere*, 84: 1175-1180.
- Arora, S., 2014. Textile dyes: It's impact on environment and its treatment. *Journal of Bioremediation & Biodegradation*. 5:e146. doi: 10.4172/2155-6199.1000e146.
- Bagal, M. V. and Gogate, P. R., 2014. Wastewater treatment using hybrid treatment schemes based on cavitation and Fenton chemistry: A review. *Ultrasonics Sonochemistry*, 21: 1-14.
- Bailey, S.E., Plin, T.J., Bricka, R.M., and Adrain, D.D., 1999. A review of potentially low cost sorbents for heavy metals. *Water Research*, 33: 2469-2479.
- Benatti, C. T. and Tavares, C. R. G., 2012. Fenton's process for the treatment of mixed waste chemicals, organic pollutants ten years after the Stockholm convention - Environmental and Analytical Update, Dr. Tomasz Puzyn (Ed.), ISBN: 978-953-307-917-2, InTech, Available from: <http://cdn.intechopen.com/pdfs-wm/29376.pdf>
- Boyter, H. A., 2007. Environmental legislations USA. In: Christie, R. (Ed.), *Environmental aspects of textile dyeing*. Woodhead, Cambridge, England, pp. 30-43.
- Braeutigam, P., Wu, Z., Stark, A. and Ondruschka, B., 2009. Degradation of BTEX in aqueous solution by hydrodynamic cavitation. *Chemical Engineering & Technology*. 32 (5): 745-753.
- Braeutigam, P., Franke, M., Schneider, R. J., Lehmann, A., Stolle, A. and Ondruschka, B., 2012. Degradation of carbamazepine in environmentally relevant concentrations in water by Hydrodynamic-Acoustic-Cavitation (HAC). *Water Research*, 46 (7): 2469-2477.
- Davis, M. and Cornwell, D.. *Introduction to Environmental Engineering 4th Edition*. New York: McGraw-Hill Science/Engineering/Math, 2006. Print.
- US Environmental Protection Agency. May 1978. *Textile Dyeing Wastewaters: Characterization and Treatment*. Environmental Protection Technology Series.

- US Environmental Protection Agency. Dec 1998. Advanced Photochemical Oxidation Processes Handbook.
- Fenton, H. J. H., 1894. Oxidation of Tartaric Acid in Presence of Iron. *Journal of the Chemical Society, Transactions*, 65 (65): 899-911.
- Glaze, W., Kang, J. W. and Chapin, D. H., 1987. The Chemistry of Water Treatment Processes Involving Ozone, Hydrogen Peroxide and Ultraviolet Radiation. *Ozone: Science & Engineering: The Journal of the International Ozone Association* 9 (4): 335-352. doi:10.1080/01919518708552148.
- Gogate, P. R. and Pandit A. B., 2001. Hydrodynamic Cavitation Reactors: A State of The Art Review. *Reviews in Chemical Engineering*, 17 (1): 1-85.
- Gore, M. M., Saharan, V. K., Pinjari, D. V., Chavan, P. V. and Pandit, A. B., 2014. Degradation of Reactive Orange 4 Dye Using Hydrodynamic Cavitation Based Hybrid Techniques. *Ultrasonics Sonochemistry*, 1075-1082.
- Hardin, I. R., 2007. Chemical Treatment of Textile dye Effluent. In: Christie, R. (Ed.), *Environmental aspects of textile dyeing*. Woodhead, Cambridge, England, pp. 193-211.
- Hypodermic Needle Gauge Chart. Retrieved March 20, 2012, from Medical Tube Technology, Inc.: [http://www.medtube.com/hypo\\_chrt.htm](http://www.medtube.com/hypo_chrt.htm).
- Jain, R., Mathur, M., Sikarwar, S., and Mittal, A., 2007. Removal of the Hazardous Dye Rhodamine B Through Photocatalytic and Adsorption Treatments. *Journal of Environmental Management*, 85 (4): 956-964.
- Kandelbuer, A., Cavaco-paulo, A. and Gubitz, G. M., 2007. Biotechnological Treatment of Textile Dye Effluent. In: Christie, R. (Ed.), *Environmental aspects of textile dyeing*. Woodhead, Cambridge, England, pp. 212-231.
- Kumar, S. S., Muruganandham, T. and Jaabir, M., 2014. Decolourization of Azo Dyes in a Two-stage Process Using Novel Isolate and Advanced Oxidation with Hydrogen Peroxide / HRP System. *International Journal of Current Microbiology and Applied Sciences*, 3 (1): 514-522.
- Kusic, H., Koprivanac, N. and Srsan, L., 2006. Azo Dye Degradation Using Fenton Type Processes Assisted by UV Irradiation: A Kinetic Study. *Journal of Photochemistry and Photobiology A-Chemistry*, 181 (2-3): 195-202.
- Leong, T., Ashokkumar, M. and Kentish, S., 2011. The Fundamentals of Power Ultrasound-A Review. *Acoustics Australia*, 39 (2): 54-63.

- Lin, S. and Chen, M., 1997. Treatment of Textile Wastewater by Chemical Methods for Reuse. *Water Research*, 31 (4): 868-876.
- Mandal, S. C., Mandal, V. and Das, A. K., 2015. *Essentials of Botanical Extraction: Principles and Applications* 1st Edition. Academic Press. pp. 96.
- Merouani, S., Hamdaoui, O., Saoudi, F., and Chiha, M., 2010. Sonochemical Degradation of Rhodamine B in Aqueous Phase: Effects of Additives. *Chemical Engineering Journal*, 158 (3): 550-557.
- Mishra, K. P. and Gogate, P. R., 2010. Intensification of Degradation of Rhodamine B Using Hydrodynamic Cavitation in the Presence of Additives. *Separation and Purification Technology*, 75 (3): 385-391.
- Munter, R., 2001. Advanced Oxidation Processes—Current Status and Prospects. *Proceedings of the Estonian Academy of Sciences. Chemistry*, 50 (2): 59-80.
- National Water Research Institute, 2000. *Treatment Technologies for Removal of Methyl Tertiary Butyl Ether (MTBE) from Drinking Water: Chapter III Advanced Oxidation Processes*.
- Needle gauge comparison chart. Retrieved November 19, 2015, from Wikipedia: [https://en.wikipedia.org/wiki/Needle\\_gauge\\_comparison\\_chart](https://en.wikipedia.org/wiki/Needle_gauge_comparison_chart)
- Nicolae, V., Sato, C., and Shields, M. S., 2009, November 5-6. Water Disinfection with In-series Ultrasound-Ultraviolet Light Reactor. 14th Intermountain Conference on the Environment & 42nd Engineering Geology and Geotechnical Engineering Symposium, Pocatello, Idaho.
- Nordin, N., Amir, S., Riyanto, and Othman, M., 2013. Textile Industries Wastewater Treatment by Electrochemical Oxidation Technique Using Metal Plate. *International Journal of Electrochemical Science*, 8: 11403-11415.
- Ogugbue, C. J. and Sawidis, T. Bioremediation and Detoxification of Synthetic Wastewater Containing Triarylmethane Dyes by *Aeromonas hydrophila* Isolated from Industrial Effluent. *Biotechnology Research International* 2011; DOI 10.4061/2011/967925.
- Patil, P. N. and Gogate, P. R., 2012. Degradation of Methyl Parathion Using Hydrodynamic Cavitation: Effect of Operating Parameters and Intensification Using Additives. *Separation and Purification Technology*, 95: 172-179.
- Pereira, L. and Alves, M., 2012. Dyes-Environmental Impact and Remediation. In Malik, A. and Grohmann, E. (Ed.), *Environmental Protection Strategies for Sustainable Development*. Springer, Netherlands, pp. 111-162.

- Pouliquen, H., Algoet, M., Buchet, V. and Le Bris, H., 1995. Acute toxicity of fluorescein to turbot (*Scophthalmus maximus*). *Veterinary and Human Toxicology* 37:527-529.
- Robinson, T., McMullan, G., Marchant, R. and Nigam, P., 2001. Remediation of dyes in textile effluent: a critical review on current treatment technologies with a proposed alternative. *Bioresource Technology*, 77 (3): 247-255.
- Saharan, V. K., Badve, M. P. and Pandit, A. B., 2011. Degradation of Reactive Red 120 Dye Using Hydrodynamic Cavitation. *Chemical Engineering Journal*, 178: 100-107.
- Sato, C. and Yao, J., 2006. Simultaneous and Sequential Photolysis of TCE and PCE. *Journal of Environmental Engineering*, 132 (1): 32-41.
- Shah, Y.T., Pandit, A.B. and Moholkar, V.S. *Cavitation Reaction Engineering*. The Plenum Chemical Engineering Series. New York: Springer US, 1999. Print.
- Sivakumar, M. and Pandit, A. B., 2001. Ultrasound Enhanced Degradation of Rhodamine B: Optimization With Power Density. *Ultrasonics Sonochemistry*, 8 (3): 233-240.
- Sivakumar, M. and Pandit, A. B., 2002. Wastewater Treatment: a Novel Energy Efficient Hydrodynamic Cavitation Technique. *Ultrasonics Sonochemistry*, 9 (3): 123-131.
- Snoeyink, V. and Jenkins, D.. *Water Chemistry* 1st Edition. Hoboken: Wiley, 1980. Print
- Suslick, K. S., Mdleleni, M. M. and Ries, J. T., 1997. Chemistry Induced by Hydrodynamic Cavitation. *Journal of the American Chemical Society*, 119 (39): 9303-9304.
- Sutkar, V. S. and Gogate, P. R., 2009. Design Aspects of Sonochemical Reactors: Techniques for Understanding Cavitation Activity Distribution and Effect of Operating Parameters. *Chemical Engineering Journal*, 155 (1-2): 26-36.
- Syringe Needle Gauge Chart. Retrieved March 20, 2012, from Sigma Aldrich: [http://www. sigmaaldrich.com/chemistry/stockroom-reagents/learning-center/technical-library/needle-gauge-chart.html](http://www.sigmaaldrich.com/chemistry/stockroom-reagents/learning-center/technical-library/needle-gauge-chart.html)
- Taylor, P. W. and Hanson, K. C., 2010. Sub-lethal Effects of Fluorescein Dye on Smoltification of Steelhead. U.S. Fish & Wildlife Service. Abernathy Fish Technology Center. Longview, WA. pp. 1-10.
- Thorneycroft, J. and Barnaby, S.W., 1895. Torpedo-boat Destroyers. *Institution of Civil Engineering*. 122: 51.

- Wang, X., Wang, J., Guo, P., Guo, W. and Li, G., 2008. Chemical Effect of Swirling Jet-induced Cavitation: Degradation of Rhodamine B in Aqueous Solution. *Ultrasonic Sonochemistry*, 15 (4): 357-363.
- Wang, X., Zhang, S. and Li, S., 2009. Decolorization of Reactive Brilliant Red K-2BP in Aqueous Solution by Using Hydrodynamic Cavitation. *Environmental Engineering Science*, 26 (1): 53-59.
- Wang, X. and Zhang, Y., 2009. Degradation of Alachlor in Aqueous Solution by Using Hydrodynamic Cavitation. *Journal of Hazardous Materials*, 161 (1): 202-207.
- Wang, J., Wang, X., Guo, P., and Yu, J., 2011a. Degradation of Reactive Brilliant red K-2BP in Aqueous Solution Using Swirling Jet-Induced Cavitation Combined With H<sub>2</sub>O<sub>2</sub> Ultrasonics *Sonochemistry*, 18 (2): 494-500.
- Wang, Z., Xue, M., Huang, K. and Liu, Z., 2011b. Textile Dyeing Wastewater Treatment, *Advances in Treating Textile Effluent*, Prof. Peter Hauser (Ed.), ISBN: 978-953-307-704-8, InTech, Available from: <http://www.intechopen.com/books/advances-in-treating-textile-effluent/textile-dyeing-wastewatertreatment>
- Wilson, K. N., 2011. Evaluation of Dispersion in Reactor With In-series Ultrasound and Ultraviolet Light. Master Thesis. Idaho State University.
- Wu, Z., Ondruschka, B., and Brautigam, P., 2007. Degradation of Chlorocarbons Driven by Hydrodynamic Cavitation. *Chemical Engineering & Technology*, 30 (5): 642-648.
- Wu, Z., Franke, M., Ondruschka, B., Zhang, Y., Ren, Y., Braeutigam, P. and Wang, W., 2011. Enhanced Effect of Suction-Cavitation on the Ozonation of Phenol. *Journal of Hazardous Materials*, 190 (1-3): 375-380.
- Wu, Z., Shen, H., Ondruschka, B., Zhang, Y., Wang, W. and Bremner, D. H. 2012. Removal of Blue-green Algae Using The Hybrid Method of Hydrodynamic Cavitation and Ozonation. *Journal of Hazardous Materials*, 235: 152-158.
- Xu, X., Li, H., Wang, W. and Gu, J., 2004. Degradation of Dyes in Aqueous Solutions by The Fenton Process. *Chemosphere*, 57: 595-600.
- Yikrazuul, 2008. Retrieved September 29, 2015, from Wikipedia: [https://en.wikipedia.org/wiki/Rhodamine\\_B](https://en.wikipedia.org/wiki/Rhodamine_B)

## Appendix A. UV-vis-spectrophotometer Calibration

### A-1. Preparation of Rhodamine B Standard Solutions

Standard solutions were made from diluting rhodamine B stock solution with DI water. Standard solutions for the high initial concentration experiments and the low initial concentration experiments were made at different time according to the following procedures.

1. Standard Solution for Low Initial Concentration Experiments
  - a. A 1.00 g/L stock solution was obtained with dissolving 0.10 g reagent grade rhodamine B into 100 ml DI water. 1 ml stock solution was then diluted into 100ml solution with a concentration of  $1.00 \times 10^{-2}$  g/L (Dilution I).
  - b. The concentrations of rhodamine B standard solution and the volume ratios of the Dilution I solution to DI water are summarized in the following Table 1.

Table A-1.1 Rhodamine B standard solution for low initial concentration experiment

Standard ID	mL of Dilution I Solution Diluted to 50 ml with DI Water	Total Volume, ml	Concentration of Rhodamine B Standards, mg/L	Concentration of Rhodamine B Standards, mM
1	0.20	50	0.04	$8.35 \times 10^{-5}$
2	0.60	50	0.12	$2.51 \times 10^{-4}$
3	1.00	50	0.20	$4.18 \times 10^{-4}$
4	3.00	50	0.60	$1.25 \times 10^{-3}$
5	4.00	50	0.80	$1.67 \times 10^{-3}$
6	6.50	50	1.30	$2.71 \times 10^{-3}$

2. Standard Solution for High Initial Concentration Experiments
  - a. A 0.80 g/L stock solution was obtained with dissolving 0.20 g reagent grade rhodamine B into 250 ml DI water. 10 ml stock solution was then diluted into 100ml solution with a concentration of  $8.00 \times 10^{-2}$  g/L (Dilution I).
  - b. The concentrations of rhodamine B standard solution and the volume ratios of the Dilution I solution to DI water are summarized in the following Table 1.

Table A-1.2 Rhodamine B standard solution for high initial concentration experiment

Standard ID	mL of Dilution I Solution Diluted to 50 ml with DI Water	Total Volume, ml	Concentration of Rhodamine B Standards, mg/L	Concentration of Rhodamine B Standards, mM
1	1.50	50	2.40	$5.01 \times 10^{-3}$
2	2.00	50	3.20	$6.68 \times 10^{-3}$
3	2.50	50	4.00	$8.35 \times 10^{-3}$
4	3.00	50	4.80	$1.00 \times 10^{-2}$
5	3.50	50	5.60	$1.17 \times 10^{-2}$
6	4.00	50	6.40	$1.34 \times 10^{-2}$

## **A-2. Calibration of UV Spectrophotometer**

1. Turn on a UV spectrophotometer, monitor, computer, and printer.
  - a. The computer performs Electronics Self-Tests: while the tests are in progress, the BUSY indicator is lit along with the POWER indicator.
  - b. The computer performs Optics Self-Tests: during the optics self-test the optical shutter will click several times. If the optics passes the self-test, the BUSY indicator should turn off leaving only the POWER and LAMP indicators on. If the optics fails, the BUSY indicator will turn off but the ERROR indicator will turn on or some combination of the LAMP, BUSY and ERROR indicators will start to flash.
2. Lamp Warm-Up: Allow the spectrophotometer lamp to warm up for at least 45 minutes.
3. Operate the UV/visible spectrophotometer from the computer monitor.
  - a. Crick CANCEL for pass ward (No pass ward is assigned).
  - b. Start the UV-Visble ChemSation scanning software by click on the icon, if is not activated by itself.
  - c. Set the system to default (choose Set Defaults from the Method menu).
4. Blank: Place a cuvette (cell) containing a blank (DI Water) solution in the cell holder.
  - a. Make sure the sample cell is oriented correctly. The frosted (non-clear) sides of the sample cell should not be in the path of the light beam.
  - b. Pushing down a lever to lock in the cell.
5. From the menu, choose MEASURE, then select Blank.
6. You will see a blank spectrum at Absorbance ~0.
7. Fill the cuvette with the standard solution having the lowest rhodamine B concentration (Part A)
8. Place a cuvette (cell) containing a standard solution in the cell holder.
  - a. Make sure the sample cell is oriented correctly. The frosted (non-clear) sides of the sample cell should not be in the path of the light beam.
  - b. Pushing down a lever to lock in the cell.
9. From the screen menu, choose MEASURE, then select Standard.
10. Measure the standard spectrum (choose Standard from the Measure menu)
  - a. After a spectrum is displayed, read Absorbance at 554 nm for a standard solution.
11. Repeat the steps 8-10 for all standard solutions.
  - a. Develop a standard curve; i.e., rhodamine B concentration vs. Absorbance

## **A-3. Measurement of Samples**

1. Repeat the steps 8-10 of PART B for an unknown sample solution.
  - a. From the menu, choose MEASURE, then select Sample.
  - b. After a spectrum is displayed, read Absorbance at 554 nm for unknown sample.
  - c. Determine K-2BP concentration using the standard curve developed.

## OVERVIEW: Working with Spectra

1. \_\_\_A spectra is used to look at individual point in the spectrum, to display tabular data of the spectrum, and to calculate transmittance for a sample.
2. \_\_\_Point to one of the spectra and click the right mouse button (a downward pointing arrow will appear).
3. \_\_\_Point to one of the spectra and click the left mouse button (the spectrum will get indicate that it has been selected).
4. \_\_\_Make a hardcopy of the complete view (choose PRINT VIEW from the file menu).
5. \_\_\_Calculate the transmittance spectrum of the selected absorbance spectrum (choose TRANSMITTANCE form the MATH menu). Open data table before change it transmittance.
6. \_\_\_Return to the Sample Spectra window (choose SAMPLES from the VIEW menu).
7. \_\_\_Point to a spectrum and double-click the left mouse button (a tabular data will appear)
8. \_\_\_A Spectra can be used to determine the wavelength peak and corresponding absorbance values of a spectrum.
9. \_\_\_Select a spectrum in the Sample Spectrum window.
10. \_\_\_Choose FIND PEAKS/VALLEYS from the Task menu, then choose Parameter and set sensitivity to 0.02 AU.
11. \_\_\_Choose Execute to do the calculation.

### A-4. Standard Curve

#### 1. Standard Curve for Low Initial Concentration Experiments

Table A-4.1 Standard solution and its absorbance

Standard ID	Absorbance at 554 nm	Concentration, mg/l	Concentration, mM
1	0.019287	0.04	$8.35 \times 10^{-5}$
2	0.041916	0.12	$2.51 \times 10^{-4}$
3	0.067062	0.20	$4.18 \times 10^{-4}$
4	0.161072	0.60	$1.25 \times 10^{-3}$
5	0.204712	0.80	$1.67 \times 10^{-3}$
6	0.34201	1.30	$2.71 \times 10^{-3}$

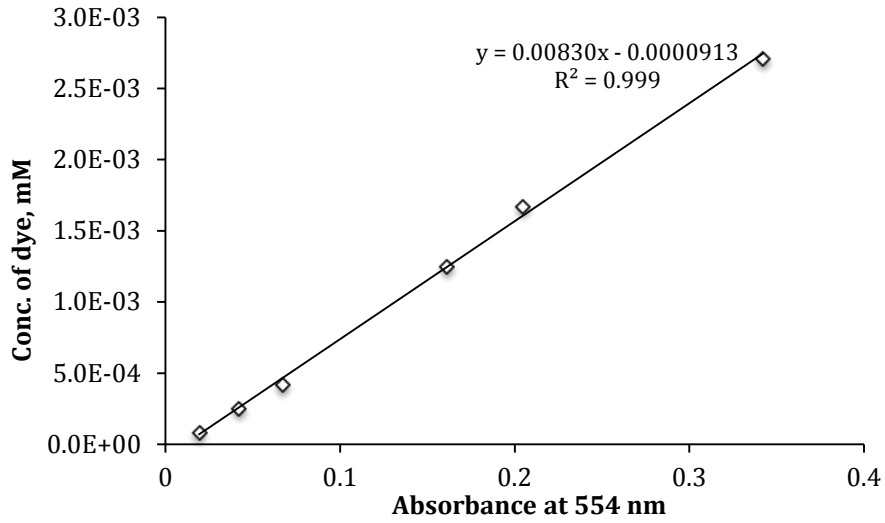


Fig. A-4.1 Calibration curve developed for low initial concentration HC experiments

## 2. Standard Curve for High Initial Concentration Experiments

Table A-4.2 Standard solution and its absorbance

Standard ID	Absorbance at 554 nm	Concentration, mg/l	Concentration, mM
1	0.49324	2.40	$5.01 \times 10^{-3}$
2	0.674835	3.20	$6.68 \times 10^{-3}$
3	0.833908	4.00	$8.35 \times 10^{-3}$
4	0.996841	4.80	$1.00 \times 10^{-2}$
5	1.154953	5.60	$1.17 \times 10^{-2}$
6	1.302307	6.40	$1.34 \times 10^{-2}$

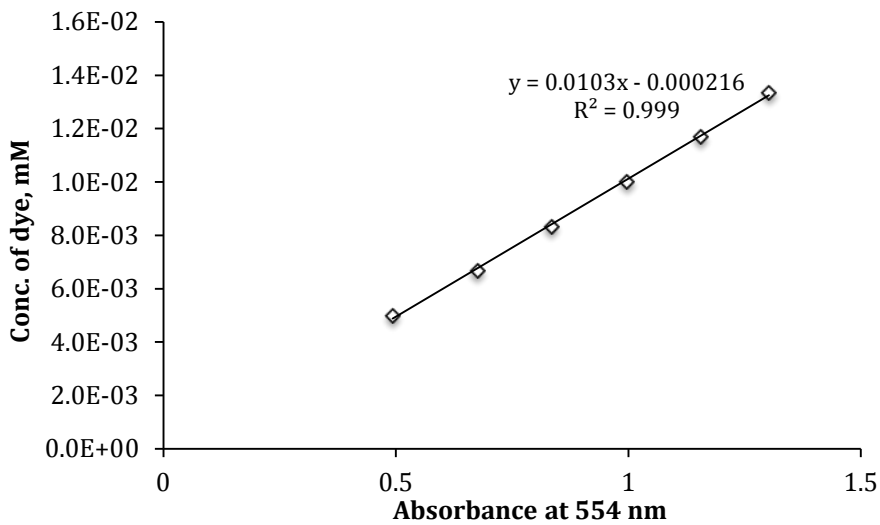


Fig. A-4.2 Calibration curve developed for high initial concentration HC experiments

### 3. Combination of Two Standard Curves

Table A-4.3 Standard solution and its absorbance

Standard ID	Absorbance at 554 nm	Concentration, mg/l	Concentration, mM
1	0.019287	0.04	$8.35 \times 10^{-5}$
2	0.041916	0.12	$2.51 \times 10^{-4}$
3	0.067062	0.20	$4.18 \times 10^{-4}$
4	0.161072	0.60	$1.25 \times 10^{-3}$
5	0.204712	0.80	$1.67 \times 10^{-3}$
6	0.34201	1.30	$2.71 \times 10^{-3}$
7	0.49324	2.40	$5.01 \times 10^{-3}$
8	0.674835	3.20	$6.68 \times 10^{-3}$
9	0.833908	4.00	$8.35 \times 10^{-3}$
10	0.996841	4.80	$1.00 \times 10^{-2}$
11	1.154953	5.60	$1.17 \times 10^{-2}$
12	1.302307	6.40	$1.34 \times 10^{-2}$

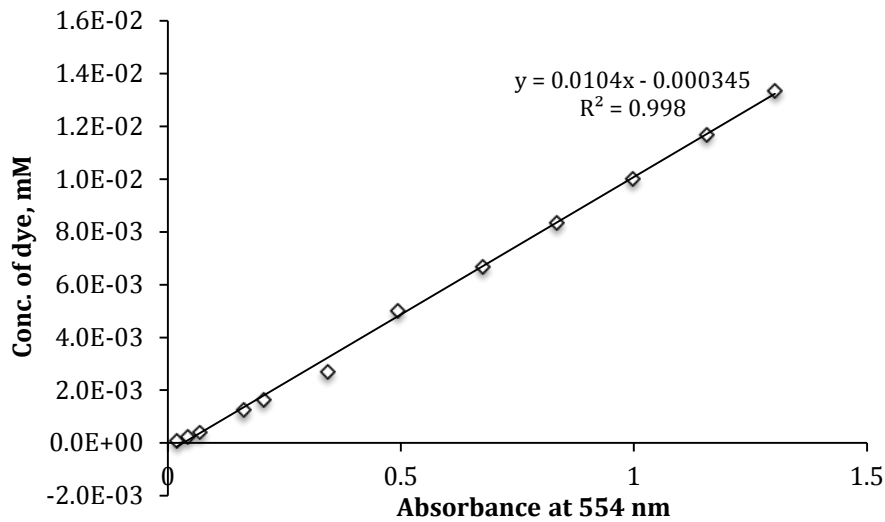


Fig. A-4.3 Calibration curve developed for AC system

### REFERENCES

- Boyd, C. E. "Water Quality" Kluwer Academic Publishers, Norwell, MA (2000).  
 Hewlett-Packard Company, "Getting Statrte with Your General Scanning Software".  
 1993.  
 Mancl, K. M. "Bacteria in drinking water". The Ohio State University Extension Service,  
 Bulletin No. 795 (1989). 63  
 Mehta, A. "Ultraviolet-Visible (UV-Vis) Spectroscopy – Principle". Analytical  
 Chemistry. Dec. 13, 2011.  
 Sato, C. Yao, J. and Ray, A. M. "Water and Wastewater Quality: a Laboratory Manual".  
 Idaho State University. (2004), 60-63

- Sivakumar, M. and Pandit, A. B. 2001. Ultrasound Enhanced Degradation of Rhodamine B: Optimization With Power Density. *Ultrasonics Sonochemistry*, 8(3): 233-240
- Sivakumar, M. and Pandit, A. B. 2002. Wastewater Treatment: a Novel Energy Efficient Hydrodynamic Cavitation Technique. *Ultrasonics Sonochemistry*, 9 (3), 123-131
- Wang, J., Wang, X., Guo, P. and Yu, J. 2011. Degradation of Reactive Brilliant red K-2BP in Aqueous Solution Using Swirling Jet-induced Cavitation Combined With  $H_2O_2$ . *Ultrasonics Sonochemistry*. 18(2): 494-500
- Wei, Y., Wang, X., Guo, W. and Wang, J. 2012. Mechanistic Study of the Degradation of Azo Dye Reactive Brilliant Red K-2BP by Ultrasound Radiation and Zero-Valent Iron. *Environmental Engineering Science*. 29(6): 399-405

## Appendix B. Original Data

### B-1. Original Data of Preliminary Study

Experimental conditions	Time	Absorbance at 554 nm wavelength	Concentration of dye based on standard curve, mM	pH	Flow rate, mL/min	Degradation rate constant, $(C_n/C_o)/t$ , $\text{min}^{-1}$
Venturi tube 1 (Model 283); $P_{in} = 50$ psi; $T = 20$ °C; $C_o = 2.51 \times 10^{-3}$ . (20150415)	0	0.183945	$1.47 \times 10^{-3}$	7.58	2051.31	0.000441 ( $R^2 = 0.831$ )
	10	0.178452	$1.42 \times 10^{-3}$	7.29		
	20	0.176224	$1.40 \times 10^{-3}$	7.40		
	30	0.17572	$1.40 \times 10^{-3}$	7.43		
	40	0.177689	$1.42 \times 10^{-3}$	7.58		
	50	0.173355	$1.38 \times 10^{-3}$	7.62		
	60	0.170166	$1.35 \times 10^{-3}$	7.64		
	70	0.172485	$1.37 \times 10^{-3}$	7.69		
	80	0.170456	$1.36 \times 10^{-3}$	7.71		
	90	0.172577	$1.37 \times 10^{-3}$	7.70		
100	0.171906	$1.37 \times 10^{-3}$	7.79			

Experimental conditions	Time	Absorbance at 554 nm wavelength	Concentration of dye based on standard curve, mM	pH	Flow rate, mL/min	Degradation rate constant, $(C_n/C_o)/t$ , $\text{min}^{-1}$
Venturi tube 1 (Model 283); $P_{in} = 60$ psi; $T = 20$ °C; $C_o = 2.51 \times 10^{-3}$ . (20150528)	0	0.154114	$1.27 \times 10^{-3}$	7.14	2048.31	0.00126 ( $R^2 = 0.963$ )
	10	0.154037	$1.27 \times 10^{-3}$	7.22		
	20	0.15889	$1.31 \times 10^{-3}$	7.58		
	30	0.156677	$1.29 \times 10^{-3}$	7.57		
	40	0.152634	$1.25 \times 10^{-3}$	7.61		
	50	0.153214	$1.26 \times 10^{-3}$	7.58		
	60	0.155975	$1.28 \times 10^{-3}$	7.64		
	70	0.149384	$1.23 \times 10^{-3}$	7.71		
	80	0.147293	$1.21 \times 10^{-3}$	7.68		
	90	0.147049	$1.21 \times 10^{-3}$	7.68		
100	0.143005	$1.17 \times 10^{-3}$	7.72			

Experimental conditions	Time	Absorbance at 554 nm wavelength	Concentration of dye based on standard curve, mM	pH	Flow rate, mL/min	Degradation rate constant, $(C_n/C_o)/t$ , $\text{min}^{-1}$
Venturi tube 1 (Model 283); $P_{in} = 70$ psi; $T = 20$ °C; $C_o = 2.51 \times 10^{-3}$ . (20150420)	0	0.178543	$1.42 \times 10^{-3}$	7.42	2583.55	0.00101 ( $R^2 = 0.943$ )
	10	0.175766	$1.40 \times 10^{-3}$	7.49		
	20	0.177124	$1.41 \times 10^{-3}$	7.54		
	30	0.174957	$1.39 \times 10^{-3}$	7.58		
	40	0.173676	$1.38 \times 10^{-3}$	7.60		
	50	0.168686	$1.34 \times 10^{-3}$	7.64		
	60	0.16925	$1.34 \times 10^{-3}$	7.68		
	70	0.163651	$1.30 \times 10^{-3}$	7.69		
	80	0.167053	$1.33 \times 10^{-3}$	7.68		
	90	0.165619	$1.31 \times 10^{-3}$	7.71		
100	0.161484	$1.28 \times 10^{-3}$	7.71			

Experimental conditions	Time	Absorbance at 554 nm wavelength	Concentration of dye based on standard curve, mM	pH	Flow rate, mL/min	Degradation rate constant, $(C_n/C_o)/t$ , $\text{min}^{-1}$
Venturi tube 2 (Model 287); $P_{in} = 50$ psi; $T = 20$ °C; $C_o = 1.20 \times 10^{-2}$ . (20150715)	0	0.876709	$8.94 \times 10^{-3}$	6.91	2970.17	0.00105 ( $R^2 = 0.880$ )
	10	0.806183	$8.21 \times 10^{-3}$	7.10		
	20	0.816254	$8.31 \times 10^{-3}$	7.12		
	30	0.79039	$8.04 \times 10^{-3}$	7.24		
	40	0.777985	$7.91 \times 10^{-3}$	7.33		
	50	0.766769	$7.79 \times 10^{-3}$	7.38		
	60	0.768707	$7.81 \times 10^{-3}$	7.40		
	70	0.735676	$7.47 \times 10^{-3}$	7.42		
	80	0.769394	$7.82 \times 10^{-3}$	7.45		
	90	0.745667	$7.57 \times 10^{-3}$	7.48		
100	0.737427	$7.49 \times 10^{-3}$	7.53			

Experimental conditions	Time	Absorbance at 554 nm wavelength	Concentration of dye based on standard curve, mM	pH	Flow rate, mL/min	Degradation rate constant, $(C_n/C_o)/t$ , $\text{min}^{-1}$
Orifice Plat 1 (One-hole); $P_{in} = 60$ psi; $T = 20$ °C; $C_o = 2.51 \times 10^{-3}$ . (20150405)	0	0.189865	$1.62 \times 10^{-3}$	7.05	1147.00	N/A
	10	0.190308	$1.62 \times 10^{-3}$	7.50		
	20	0.188324	$1.61 \times 10^{-3}$	7.65		
	30	0.18956	$1.62 \times 10^{-3}$	7.81		
	40	0.189545	$1.62 \times 10^{-3}$	7.97		
	50	0.188995	$1.61 \times 10^{-3}$	7.97		
	60	0.186905	$1.59 \times 10^{-3}$	8.05		
	70	0.18663	$1.59 \times 10^{-3}$	8.10		
	80	0.188873	$1.61 \times 10^{-3}$	8.12		
	90	0.185989	$1.59 \times 10^{-3}$	8.13		
100	0.187485	$1.60 \times 10^{-3}$	8.12			

Experimental conditions	Time	Absorbance at 554 nm wavelength	Concentration of dye based on standard curve, mM	pH	Flow rate, mL/min	Degradation rate constant, $(C_n/C_o)/t$ , $\text{min}^{-1}$
Orifice Plat 1 (One-hole); $P_{in} = 100$ psi; $T = 20$ °C; $C_o = 2.51 \times 10^{-3}$ . (20150406)	0	0.19812	$1.69 \times 10^{-3}$	7.60	1312.80	N/A
	10	0.192398	$1.64 \times 10^{-3}$	7.80		
	20	0.191895	$1.64 \times 10^{-3}$	7.98		
	30	0.194717	$1.66 \times 10^{-3}$	8.08		
	40	0.19162	$1.64 \times 10^{-3}$	8.07		
	50	0.191833	$1.64 \times 10^{-3}$	8.12		
	60	0.190063	$1.62 \times 10^{-3}$	8.12		
	70	0.196701	$1.68 \times 10^{-3}$	8.20		
	80	0.194611	$1.66 \times 10^{-3}$	8.21		
	90	0.193924	$1.66 \times 10^{-3}$	8.21		
	100	0.197662	$1.69 \times 10^{-3}$	8.22		

Experimental data for Orifice Plate 2 (Three-hole) (20150405), Needle Tube 1 (14 G) (20150605), Needle Tube 2 (14 G-2 holes) (20150605), Needle Tube 3 (18 G) (20150605), and Needle Tube 4 (18 G-a cone cape) (20150615) are not available, since no bubble was observed after tubes were full filled with experimental solution.

## B-2. Original Data for two Venturi tubes

Experimental conditions	Time	Absorbance at 554 nm wavelength	Concentration of dye based on standard curve, mM	pH	Flow rate, mL/min	Degradation rate constant, $(C_n/C_o)/t$ , $\text{min}^{-1}$
Venturi tube 1 (Model 283); $P_{in} = 70$ psi; $T = 20$ °C; $C_o = 2.51 \times 10^{-3}$ . (20150420)	0	0.178543	$1.42 \times 10^{-3}$	7.42	2583.55	0.00101 ( $R^2 = 0.943$ )
	10	0.175766	$1.40 \times 10^{-3}$	7.49		
	20	0.177124	$1.41 \times 10^{-3}$	7.54		
	30	0.174957	$1.39 \times 10^{-3}$	7.58		
	40	0.173676	$1.38 \times 10^{-3}$	7.60		
	50	0.168686	$1.34 \times 10^{-3}$	7.64		
	60	0.16925	$1.34 \times 10^{-3}$	7.68		
	70	0.163651	$1.30 \times 10^{-3}$	7.69		
	80	0.167053	$1.33 \times 10^{-3}$	7.68		
	90	0.165619	$1.31 \times 10^{-3}$	7.71		
	100	0.161484	$1.28 \times 10^{-3}$	7.71		

Experimental conditions	Time	Absorbance at 554 nm wavelength	Concentration of dye based on standard curve, mM	pH	Flow rate, mL/min	Degradation rate constant, $(C_t/C_o)/t$ , $\text{min}^{-1}$
Venturi tube 1 (Model 283); $P_{in} = 70$ psi; $T = 20$ °C; $C_o = 2.51 \times 10^{-3}$ . (20150603)	0	0.179382	$1.41 \times 10^{-3}$	6.55	2656.50	0.00121 ( $R^2 = 0.945$ )
	10	0.183105	$1.45 \times 10^{-3}$	6.96		
	20	0.17955	$1.42 \times 10^{-3}$	6.87		
	30	0.175705	$1.38 \times 10^{-3}$	7.14		
	40	0.176376	$1.39 \times 10^{-3}$	7.10		
	50	0.174225	$1.37 \times 10^{-3}$	7.16		
	60	0.171341	$1.35 \times 10^{-3}$	7.11		
	70	0.171906	$1.35 \times 10^{-3}$	7.22		
	80	0.16983	$1.33 \times 10^{-3}$	7.22		
	90	0.164047	$1.29 \times 10^{-3}$	7.21		
100	0.164154	$1.29 \times 10^{-3}$	7.25			

Experimental conditions	Time	Absorbance at 554 nm wavelength	Concentration of dye based on standard curve, mM	pH	Flow rate, mL/min	Degradation rate constant, $(C_t/C_o)/t$ , $\text{min}^{-1}$
Venturi tube 1 (Model 283); $P_{in} = 70$ psi; $T = 20$ °C; $C_o = 2.51 \times 10^{-3}$ . (20150608)	0	0.152237	$1.19 \times 10^{-3}$	6.75	2584.07	0.00118 ( $R^2 = 0.959$ )
	10	0.156708	$1.23 \times 10^{-3}$	7.15		
	20	0.156006	$1.22 \times 10^{-3}$	6.92		
	30	0.154572	$1.21 \times 10^{-3}$	6.94		
	40	0.151154	$1.18 \times 10^{-3}$	6.97		
	50	0.152161	$1.19 \times 10^{-3}$	6.95		
	60	0.147812	$1.15 \times 10^{-3}$	6.99		
	70	0.148407	$1.16 \times 10^{-3}$	7.00		
	80	0.14624	$1.14 \times 10^{-3}$	7.03		
	90	0.148865	$1.16 \times 10^{-3}$	7.05		
100	0.141724	$1.10 \times 10^{-3}$	7.07			

Experimental conditions	Time	Absorbance at 554 nm wavelength	Concentration of dye based on standard curve, mM	pH	Flow rate, mL/min	Degradation rate constant, $(C_t/C_o)/t$ , $\text{min}^{-1}$
Venturi tube 1 (Model 283); $P_{in} = 70$ psi; $T = 20$ °C; $C_o = 2.51 \times 10^{-3}$ . (20150612)	0	0.20546	$1.63 \times 10^{-3}$	6.49	2682.53	0.00109 ( $R^2 = 0.820$ )
	10	0.215424	$1.72 \times 10^{-3}$	6.56		
	20	0.208099	$1.65 \times 10^{-3}$	6.59		
	30	0.201935	$1.60 \times 10^{-3}$	6.61		
	40	0.206711	$1.64 \times 10^{-3}$	6.54		
	50	0.199799	$1.58 \times 10^{-3}$	6.75		
	60	0.198853	$1.58 \times 10^{-3}$	6.80		
	70	0.194183	$1.54 \times 10^{-3}$	6.80		
	80	0.195343	$1.55 \times 10^{-3}$	6.77		
	90	0.195709	$1.55 \times 10^{-3}$	6.78		
100	0.19455	$1.54 \times 10^{-3}$	6.82			

Experimental conditions	Time	Absorbance at 554 nm wavelength	Concentration of dye based on standard curve, mM	pH	Flow rate, mL/min	Degradation rate constant, $(C_t/C_o)/t$ , $\text{min}^{-1}$
Venturi tube 1 (Model 283); $P_{in} = 70$ psi; $T = 20$ °C; $C_o = 1.20 \times 10^{-2}$ . (20150619)	0	0.904175	$9.23 \times 10^{-3}$	7.09	2675.88	0.000553 ( $R^2 = 0.910$ )
	10	0.91658	$9.36 \times 10^{-3}$	7.16		
	20	0.905991	$9.25 \times 10^{-3}$	7.22		
	30	0.903473	$9.22 \times 10^{-3}$	7.23		
	40	0.891708	$9.10 \times 10^{-3}$	7.27		
	50	0.893433	$9.12 \times 10^{-3}$	7.39		
	60	0.876831	$8.94 \times 10^{-3}$	7.37		
	70	0.880371	$8.98 \times 10^{-3}$	7.42		
	80	0.878235	$8.96 \times 10^{-3}$	7.37		
	90	0.874313	$8.92 \times 10^{-3}$	7.41		
100	0.872482	$8.90 \times 10^{-3}$	7.43			

Experimental conditions	Time	Absorbance at 554 nm wavelength	Concentration of dye based on standard curve, mM	pH	Flow rate, mL/min	Degradation rate constant, $(C_i/C_o)/t$ , min <sup>-1</sup>
Venturi tube 1 (Model 283); $P_{in} = 70$ psi; $T = 20$ °C; $C_o = 1.20 \times 10^{-2}$ . (20150708)	0	0.950897	$9.72 \times 10^{-3}$	6.85	2395.46	0.000369 ( $R^2 = 0.736$ )
	10	0.973648	$9.95 \times 10^{-3}$	7.00		
	20	0.978546	$1.00 \times 10^{-3}$	7.12		
	30	0.961166	$9.82 \times 10^{-3}$	7.16		
	40	0.963165	$9.84 \times 10^{-3}$	7.29		
	50	0.968155	$9.90 \times 10^{-3}$	7.17		
	60	0.948593	$9.69 \times 10^{-3}$	7.27		
	70	0.949127	$9.70 \times 10^{-3}$	7.23		
	80	0.959396	$9.81 \times 10^{-3}$	7.27		
	90	0.942841	$9.63 \times 10^{-3}$	7.25		
100	0.945724	$9.66 \times 10^{-3}$	7.29			

Experimental conditions	Time	Absorbance at 554 nm wavelength	Concentration of dye based on standard curve, mM	pH	Flow rate, mL/min	Degradation rate constant, $(C_i/C_o)/t$ , min <sup>-1</sup>
Venturi tube 1 (Model 283); $P_{in} = 70$ psi; $T = 20$ °C; $C_o = 1.20 \times 10^{-2}$ . (20150713)	0	0.90361	$9.22 \times 10^{-3}$	6.64	2406.34	0.000523 ( $R^2 = 0.903$ )
	10	0.910736	$9.30 \times 10^{-3}$	7.02		
	20	0.906006	$9.25 \times 10^{-3}$	7.13		
	30	0.904526	$9.23 \times 10^{-3}$	7.22		
	40	0.896118	$9.14 \times 10^{-3}$	7.25		
	50	0.898621	$9.17 \times 10^{-3}$	7.26		
	60	0.895905	$9.14 \times 10^{-3}$	7.37		
	70	0.900467	$9.19 \times 10^{-3}$	7.40		
	80	0.873596	$8.91 \times 10^{-3}$	7.38		
	90	0.876434	$8.94 \times 10^{-3}$	7.47		
100	0.85463	$8.71 \times 10^{-3}$	7.46			

Experimental conditions	Time	Absorbance at 554 nm wavelength	Concentration of dye based on standard curve, mM	pH	Flow rate, mL/min	Degradation rate constant, $(C_i/C_o)/t$ , min <sup>-1</sup>
Venturi tube 2 (Model 287); $P_{in} = 55$ psi; $T = 20$ °C; $C_o = 1.20 \times 10^{-2}$ . (20150808)	0	0.884323	$9.02 \times 10^{-3}$	6.32	3189.05	0.0006582 ( $R^2 = 0.734$ )
	10	0.863052	$8.80 \times 10^{-3}$	6.26		
	20	0.826126	$8.41 \times 10^{-3}$	6.27		
	30	0.829193	$8.45 \times 10^{-3}$	6.22		
	40	0.821243	$8.36 \times 10^{-3}$	6.28		
	50	0.819702	$8.35 \times 10^{-3}$	6.27		
	60	0.807739	$8.22 \times 10^{-3}$	6.28		
	70	0.804687	$8.19 \times 10^{-3}$	6.29		
	80	0.80629	$8.21 \times 10^{-3}$	6.29		
	90	0.792267	$8.06 \times 10^{-3}$	6.33		
100	0.808426	$8.23 \times 10^{-3}$	6.33			

Experimental conditions	Time	Absorbance at 554 nm wavelength	Concentration of dye based on standard curve, mM	pH	Flow rate, mL/min	Degradation rate constant, $(C_i/C_o)/t$ , min <sup>-1</sup>
Venturi tube 2 (Model 287); $P_{in} = 55$ psi; $T = 20$ °C; $C_o = 1.20 \times 10^{-2}$ . (20150809)	0	0.887375	$9.05 \times 10^{-3}$	6.60	3354.53	0.000532 ( $R^2 = 0.826$ )
	10	0.869202	$8.86 \times 10^{-3}$	6.53		
	20	0.87825	$8.96 \times 10^{-3}$	6.50		
	30	0.861969	$8.79 \times 10^{-3}$	6.49		
	40	0.875198	$8.93 \times 10^{-3}$	6.45		
	50	0.864868	$8.82 \times 10^{-3}$	6.41		
	60	0.84845	$8.65 \times 10^{-3}$	6.40		
	70	0.850082	$8.66 \times 10^{-3}$	6.48		
	80	0.855072	$8.72 \times 10^{-3}$	6.46		
	90	0.83786	$8.54 \times 10^{-3}$	6.39		
100	0.839767	$8.56 \times 10^{-3}$	6.45			

Experimental conditions	Time	Absorbance at 554 nm wavelength	Concentration of dye based on standard curve, mM	pH	Flow rate, mL/min	Degradation rate constant, $(C_t/C_o)/t$ , $\text{min}^{-1}$
Venturi tube 2 (Model 287); $P_{in} = 55$ psi; $T = 20$ °C; $C_o = 1.20 \times 10^{-2}$ . (20150810)	0	0.987183	$1.01 \times 10^{-2}$	6.74	3173.42	0.00109 ( $R^2 = 0.853$ )
	10	0.976334	$9.98 \times 10^{-3}$	6.55		
	20	0.984314	$1.01 \times 10^{-2}$	6.66		
	30	0.952057	$9.73 \times 10^{-3}$	6.54		
	40	0.930069	$9.50 \times 10^{-3}$	6.50		
	50	0.914581	$9.34 \times 10^{-3}$	6.44		
	60	0.927811	$9.48 \times 10^{-3}$	6.43		
	70	0.920242	$9.40 \times 10^{-3}$	6.38		
	80	0.88855	$9.07 \times 10^{-3}$	6.36		
	90	0.889603	$9.08 \times 10^{-3}$	6.32		
100	0.907883	$9.27 \times 10^{-3}$	6.30			

Experimental conditions	Time	Absorbance at 554 nm wavelength	Concentration of dye based on standard curve, mM	pH	Flow rate, mL/min	Degradation rate constant, $(C_t/C_o)/t$ , $\text{min}^{-1}$
Venturi tube 2 (Model 287); $P_{in} = 50$ psi; $T = 20$ °C; $C_o = 1.20 \times 10^{-2}$ . (20150715)	0	0.876709	$8.94 \times 10^{-3}$	6.91	2970.17	0.00105 ( $R^2 = 0.880$ )
	10	0.806183	$8.21 \times 10^{-3}$	7.10		
	20	0.816254	$8.31 \times 10^{-3}$	7.12		
	30	0.79039	$8.04 \times 10^{-3}$	7.24		
	40	0.777985	$7.91 \times 10^{-3}$	7.33		
	50	0.766769	$7.79 \times 10^{-3}$	7.38		
	60	0.768707	$7.81 \times 10^{-3}$	7.40		
	70	0.735676	$7.47 \times 10^{-3}$	7.42		
	80	0.769394	$7.82 \times 10^{-3}$	7.45		
	90	0.745667	$7.57 \times 10^{-3}$	7.48		
100	0.737427	$7.49 \times 10^{-3}$	7.53			

Experimental conditions	Time	Absorbance at 554 nm wavelength	Concentration of dye based on standard curve, mM	pH	Flow rate, mL/min	Degradation rate constant, $(C_t/C_o)/t$ , $\text{min}^{-1}$
Venturi tube 2 (Model 287); $P_{in} = 50$ psi; $T = 20$ °C; $C_o = 1.20 \times 10^{-2}$ . (20150716)	0	0.874512	$8.92 \times 10^{-3}$	6.97	3003.96	0.00143 ( $R^2 = 0.921$ )
	10	0.859726	$8.77 \times 10^{-3}$	7.09		
	20	0.840317	$8.56 \times 10^{-3}$	7.20		
	30	0.827255	$8.43 \times 10^{-3}$	7.29		
	40	0.818817	$8.34 \times 10^{-3}$	7.35		
	50	0.824799	$8.40 \times 10^{-3}$	7.43		
	60	0.815247	$8.30 \times 10^{-3}$	7.47		
	70	0.809174	$8.24 \times 10^{-3}$	7.48		
	80	0.788544	$8.02 \times 10^{-3}$	7.48		
	90	0.756088	$7.68 \times 10^{-3}$	7.47		
100	0.748856	$7.61 \times 10^{-3}$	7.50			

Experimental conditions	Time	Absorbance at 554 nm wavelength	Concentration of dye based on standard curve, mM	pH	Flow rate, mL/min	Degradation rate constant, $(C_t/C_o)/t$ , $\text{min}^{-1}$
Venturi tube 2 (Model 287); $P_{in} = 50$ psi; $T = 20$ °C; $C_o = 1.20 \times 10^{-2}$ . (20150728)	0	0.891891	$9.10 \times 10^{-3}$	6.26	2998.39	0.000857 ( $R^2 = 0.921$ )
	10	0.894562	$9.13 \times 10^{-3}$	6.37		
	20	0.87294	$8.90 \times 10^{-3}$	6.95		
	30	0.843872	$8.60 \times 10^{-3}$	7.09		
	40	0.858154	$8.75 \times 10^{-3}$	7.18		
	50	0.831009	$8.47 \times 10^{-3}$	7.23		
	60	0.836899	$8.53 \times 10^{-3}$	7.28		
	70	0.833328	$8.49 \times 10^{-3}$	7.32		
	80	0.84285	$8.59 \times 10^{-3}$	7.41		
	90	0.834732	$8.50 \times 10^{-3}$	7.42		
100	0.818634	$8.34 \times 10^{-3}$	7.46			

Experimental conditions	Time	Absorbance at 554 nm wavelength	Concentration of dye based on standard curve, mM	pH	Flow rate, mL/min	Degradation rate constant, $(C_t/C_o)/t$ , min <sup>-1</sup>
Venturi tube 2 (Model 287); $P_{in} = 40$ psi; $T = 20$ °C; $C_o = 1.20 \times 10^{-2}$ . (20150731)	0	0.925034	9.45E-06	6.05	2718.48	0.000820 ( $R^2 = 0.882$ )
	10	0.866776	$8.84 \times 10^{-3}$	6.12		
	20	0.95285	$9.74 \times 10^{-3}$	6.19		
	30	0.894714	$9.13 \times 10^{-3}$	6.21		
	40	0.858994	$8.76 \times 10^{-3}$	6.30		
	50	0.874237	$8.92 \times 10^{-3}$	6.29		
	60	0.893066	$9.11 \times 10^{-3}$	6.30		
	70	0.877335	$8.95 \times 10^{-3}$	6.30		
	80	0.859146	$8.76 \times 10^{-3}$	6.31		
	90	0.897568	$9.16 \times 10^{-3}$	6.35		
100	0.850067	$8.66 \times 10^{-3}$	6.21			

Experimental conditions	Time	Absorbance at 554 nm wavelength	Concentration of dye based on standard curve, mM	pH	Flow rate, mL/min	Degradation rate constant, $(C_t/C_o)/t$ , min <sup>-1</sup>
Venturi tube 2 (Model 287); $P_{in} = 40$ psi; $T = 20$ °C; $C_o = 1.20 \times 10^{-2}$ . (20150803)	0	0.842499	$8.59 \times 10^{-3}$	5.93	2776.05	0.000882 ( $R^2 = 0.927$ )
	10	0.848358	$8.65 \times 10^{-3}$	6.02		
	20	0.854431	$8.71 \times 10^{-3}$	6.10		
	30	0.790161	$8.04 \times 10^{-3}$	6.15		
	40	0.785568	$7.99 \times 10^{-3}$	6.23		
	50	0.813324	$8.28 \times 10^{-3}$	6.25		
	60	0.791687	$8.05 \times 10^{-3}$	6.29		
	70	0.80368	$8.18 \times 10^{-3}$	6.27		
	80	0.793015	$8.07 \times 10^{-3}$	6.30		
	90	0.822754	$8.38 \times 10^{-3}$	6.33		
100	0.778168	$7.91 \times 10^{-3}$	6.35			

Experimental conditions	Time	Absorbance at 554 nm wavelength	Concentration of dye based on standard curve, mM	pH	Flow rate, mL/min	Degradation rate constant, $(C_t/C_o)/t$ , min <sup>-1</sup>
Venturi tube 2 (Model 287); $P_{in} = 40$ psi; $T = 20$ °C; $C_o = 1.20 \times 10^{-2}$ . (20150816)	0	0.888565	$9.07 \times 10^{-3}$	N/A	2766.53	0.00112 ( $R^2 = 0.800$ )
	5	0.887848	$9.06 \times 10^{-3}$			
	10	0.90799	$9.27 \times 10^{-3}$			
	15	0.904877	$9.24 \times 10^{-3}$			
	20	0.903549	$9.22 \times 10^{-3}$			
	25	0.89212	$9.10 \times 10^{-3}$			
	30	0.913086	$9.32 \times 10^{-3}$			
	35	0.901596	$9.20 \times 10^{-3}$			
	40	0.876816	$8.94 \times 10^{-3}$			
	45	0.904816	$9.24 \times 10^{-3}$			
	50	0.891617	$9.10 \times 10^{-3}$			
	55	0.855591	$8.72 \times 10^{-3}$			
	60	0.836578	$8.52 \times 10^{-3}$			
	65	0.867218	$8.84 \times 10^{-3}$			
	70	0.867813	$8.85 \times 10^{-3}$			
	75	0.830643	$8.46 \times 10^{-3}$			
	80	0.844894	$8.61 \times 10^{-3}$			
	85	0.851349	$8.68 \times 10^{-3}$			
90	0.832306	$8.48 \times 10^{-3}$				
95	0.833862	$8.50 \times 10^{-3}$				
100	0.868774	$8.86 \times 10^{-3}$				

Experimental conditions	Time	Absorbance at 554 nm wavelength	Concentration of dye based on standard curve, mM	pH	Flow rate, mL/min	Degradation rate constant, $(C_t/C_o)/t$ , $\text{min}^{-1}$
Venturi tube 2 (Model 287); $P_{in} = 30$ psi; $T = 20$ °C; $C_o = 1.20 \times 10^{-2}$ . (20150816)	0	0.858856	$8.76 \times 10^{-3}$	6.93	2439.85	0.000661 ( $R^2 = 0.881$ )
	5	0.86499	$8.82 \times 10^{-3}$	6.96		
	10	0.859833	$8.77 \times 10^{-3}$	6.96		
	15	0.848343	$8.65 \times 10^{-3}$	6.96		
	20	0.854904	$8.71 \times 10^{-3}$	6.88		
	25	0.854996	$8.72 \times 10^{-3}$	6.83		
	30	0.854721	$8.71 \times 10^{-3}$	6.86		
	35	0.847076	$8.63 \times 10^{-3}$	6.83		
	40	0.840271	$8.56 \times 10^{-3}$	6.82		
	45	0.857788	$8.74 \times 10^{-3}$	6.81		
	50	0.844208	$8.60 \times 10^{-3}$	6.86		
	55	0.823929	$8.39 \times 10^{-3}$	6.84		
	60	0.827942	$8.43 \times 10^{-3}$	6.84		
	65	0.820877	$8.36 \times 10^{-3}$	7.14		
	70	0.820831	$8.36 \times 10^{-3}$	7.18		
	75	0.820679	$8.36 \times 10^{-3}$	7.15		
	80	0.836823	$8.53 \times 10^{-3}$	7.10		
85	0.835037	$8.51 \times 10^{-3}$	7.04			
90	0.808685	$8.23 \times 10^{-3}$	6.98			
95	0.808029	$8.23 \times 10^{-3}$	6.99			
100	0.811066	$8.26 \times 10^{-3}$	7.21			

Experimental conditions	Time	Absorbance at 554 nm wavelength	Concentration of dye based on standard curve, mM	pH	Flow rate, mL/min	Degradation rate constant, $(C_t/C_o)/t$ , $\text{min}^{-1}$
Venturi tube 2 (Model 287); $P_{in} = 30$ psi; $T = 20$ °C; $C_o = 1.20 \times 10^{-2}$ . (20150817)	0	0.907257	$9.26 \times 10^{-3}$	6.82	2483.71	0.000713 ( $R^2 = 0.758$ )
	5	0.877548	$8.95 \times 10^{-3}$	6.88		
	10	0.888046	$9.06 \times 10^{-3}$	6.92		
	15	0.876785	$8.94 \times 10^{-3}$	6.83		
	20	0.891113	$9.09 \times 10^{-3}$	6.88		
	25	0.873001	$8.90 \times 10^{-3}$	6.83		
	30	0.869843	$8.87 \times 10^{-3}$	6.83		
	35	0.879379	$8.97 \times 10^{-3}$	6.82		
	40	0.857468	$8.74 \times 10^{-3}$	6.82		
	45	0.858307	$8.75 \times 10^{-3}$	6.81		
	50	0.84726	$8.63 \times 10^{-3}$	6.83		
	55	0.847504	$8.64 \times 10^{-3}$	6.83		
	60	0.847061	$8.63 \times 10^{-3}$	6.87		
	65	0.845032	$8.61 \times 10^{-3}$	6.87		
	70	0.844727	$8.61 \times 10^{-3}$	6.86		
	75	0.842545	$8.59 \times 10^{-3}$	6.86		
	80	0.846176	$8.62 \times 10^{-3}$	6.87		
85	0.832596	$8.48 \times 10^{-3}$	6.92			
90	0.813629	$8.28 \times 10^{-3}$	6.92			
95	0.85321	$8.70 \times 10^{-3}$	6.91			
100	0.85405	$8.71 \times 10^{-3}$	7.11			

Experimental conditions	Time	Absorbance at 554 nm wavelength	Concentration of dye based on standard curve, mM	pH	Flow rate, mL/min	Degradation rate constant, $(C_i/C_o)/t$ , $\text{min}^{-1}$
Venturi tube 2 (Model 287); $P_{in} = 30$ psi; $T = 20$ °C; $C_o = 1.20 \times 10^{-2}$ . (20150818)	0	0.955872	$9.77 \times 10^{-3}$	6.08	2488.39	0.000603 ( $R^2 = 0.831$ )
	5	0.953766	$9.75 \times 10^{-3}$	6.74		
	10	0.936264	$9.56 \times 10^{-3}$	6.79		
	15	0.940796	$9.61 \times 10^{-3}$	6.79		
	20	0.941467	$9.62 \times 10^{-3}$	6.81		
	25	0.950867	$9.72 \times 10^{-3}$	6.79		
	30	0.932327	$9.52 \times 10^{-3}$	6.75		
	35	0.935028	$9.55 \times 10^{-3}$	6.79		
	40	0.929916	$9.50 \times 10^{-3}$	6.85		
	45	0.929932	$9.50 \times 10^{-3}$	6.78		
	50	0.931152	$9.51 \times 10^{-3}$	6.79		
	55	0.938797	$9.59 \times 10^{-3}$	6.79		
	60	0.921661	$9.41 \times 10^{-3}$	6.76		
	65	0.921585	$9.41 \times 10^{-3}$	6.75		
	70	0.907562	$9.26 \times 10^{-3}$	6.82		
	75	0.909164	$9.28 \times 10^{-3}$	6.84		
	80	0.920303	$9.40 \times 10^{-3}$	6.80		
85	0.901459	$9.20 \times 10^{-3}$	6.77			
90	0.896866	$9.15 \times 10^{-3}$	6.76			
95	0.889526	$9.08 \times 10^{-3}$	6.74			
100	0.910843	$9.30 \times 10^{-3}$	6.73			

### B-3. Original Data of AC System

Experimental conditions	ID	Initial Concentration of Rhodamine B, mM	Time, min	Measured Concentration of Effluent, mM		Flow rate, mL/min
				Absorbance at 554 nm wavelength	Concentration of dye based on standard curve, mM	
Ultrasound Horn; $T = 15-39$ °C; $C_o = 1.20 \times 10^{-2}$ .	20150702	$9.73 \times 10^{-3}$	0	0.968277	$9.73 \times 10^{-3}$	100
			8	0.931076	$9.34 \times 10^{-3}$	
			16	0.910812	$9.13 \times 10^{-3}$	
			24	0.909454	$9.11 \times 10^{-3}$	
			32	0.903168	$9.05 \times 10^{-3}$	
			40	0.899353	$9.01 \times 10^{-3}$	
			48	0.902786	$9.04 \times 10^{-3}$	
			56	0.882355	$8.83 \times 10^{-3}$	
			64	0.957214	$9.61 \times 10^{-3}$	
			72	0.885757	$8.87 \times 10^{-3}$	
			86	0.902008	$9.04 \times 10^{-3}$	
106	0.901337	$9.03 \times 10^{-3}$				

Experimental conditions	ID	Initial Concentration of Rhodamine B, mM	Time, min	Measured Concentration of Effluent, mM		Flow rate, mL/min
				Absorbance at 554 nm wavelength	Concentration of dye based on standard curve, mM	
Ultrasound Horn; T = 15-39 °C; C <sub>o</sub> = 1.20 × 10 <sup>-2</sup> .	20150707	1.12 × 10 <sup>-2</sup>	0	1.114349	1.12 × 10 <sup>-2</sup>	100
			8	1.095322	1.10 × 10 <sup>-2</sup>	
			16	1.058243	1.07 × 10 <sup>-2</sup>	
			24	1.046402	1.05 × 10 <sup>-2</sup>	
			32	1.056458	1.06 × 10 <sup>-2</sup>	
			40	1.060913	1.07 × 10 <sup>-2</sup>	
			48	1.040451	1.05 × 10 <sup>-2</sup>	
			56	1.028427	1.04 × 10 <sup>-2</sup>	
			64	1.050018	1.06 × 10 <sup>-2</sup>	
			72	1.046112	1.05 × 10 <sup>-2</sup>	
			86	1.045563	1.05 × 10 <sup>-2</sup>	
106	1.035645	1.04 × 10 <sup>-2</sup>				

Experimental conditions	ID	Initial Concentration of Rhodamine B, mM	Time, min	Measured Concentration of Effluent, mM		Flow rate, mL/min
				Absorbance at 554 nm wavelength	Concentration of dye based on standard curve, mM	
Ultrasound Horn; T = 15-39 °C; C <sub>o</sub> = 1.20 × 10 <sup>-2</sup> .	20150709	1.02 × 10 <sup>-2</sup>	0	1.018661	1.02 × 10 <sup>-2</sup>	100
			8	0.994675	1.00 × 10 <sup>-2</sup>	
			16	0.967407	9.72 × 10 <sup>-3</sup>	
			24	0.957703	9.62 × 10 <sup>-3</sup>	
			32	0.953568	9.57 × 10 <sup>-3</sup>	
			40	0.949783	9.53 × 10 <sup>-3</sup>	
			48	0.9646	9.69 × 10 <sup>-3</sup>	
			56	0.949203	9.53 × 10 <sup>-3</sup>	
			64	0.947754	9.51 × 10 <sup>-3</sup>	
			72	0.954605	9.58 × 10 <sup>-3</sup>	
			86	0.956329	9.60 × 10 <sup>-3</sup>	
106	0.963165	9.67 × 10 <sup>-3</sup>				

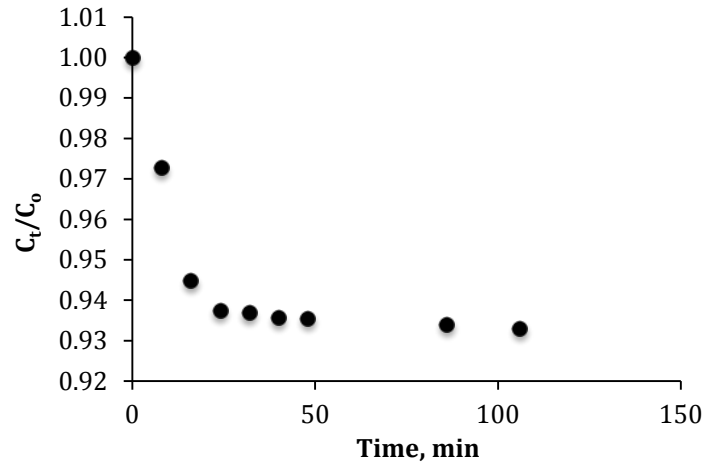
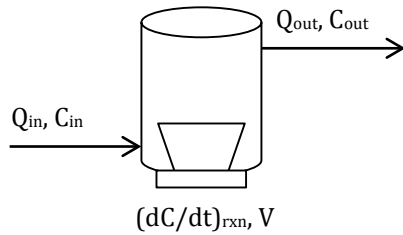
## Appendix C. Calculation

### C-1. Degradation Rate Constant of HC System

Degradation rate constants of HC system were obtained with the exponential regression equations:

- Venturi tube 1 (Model 283) with initial concentration of  $2.51 \times 10^{-3}$  ( $1.45 \times 10^{-3}$  measured value),  $C_t/C_o = 1.01e^{-0.00114t}$  ( $t = 0-100$  min),  $k = 1.14 \times 10^{-3}$ ,  $R^2 = 0.985$ ;
- Venturi tube 1 (Model 283) with initial concentration of  $1.20 \times 10^{-2}$  ( $9.49 \times 10^{-3}$  measured value),  $C_t/C_o = 1.01e^{-0.000531t}$  ( $t = 0-100$  min),  $k = 5.31 \times 10^{-4}$ ,  $R^2 = 0.966$ ;
- Venturi tube 2 (Model 287) with initial concentration of  $1.20 \times 10^{-2}$  ( $8.74 \times 10^{-3}$  measured value),  $C_t/C_o = 1.00e^{-0.00109t}$  ( $t = 0-100$  min),  $k = 1.09 \times 10^{-3}$ ,  $R^2 = 0.978$ ;

### C-2. Degradation Rate Constant of AC System



Select US chamber as a system. From the normalized dye conc. vs. time plot, after 48 min, the system turned to be at a steady state. Assume the dye degradation reaction follows first order kinetics. Do Mass Balance around US chamber:

$$\frac{dC}{dt}V = Q_{in}C_{in} - Q_{out}C - kCV \quad (Eq. C - 1)$$

Where  $C_{in}$  = dye concentration in influent (mM);  $C$  = dye concentration in effluent (mM),  $Q_{in}$  = influent flow rate (mL/min);  $Q_{out}$  = effluent flow rate (mL/min);  $V$  = reactor volume (mL);  $k$  = first-order reaction-rate constant ( $\text{min}^{-1}$ ); and  $t$  = time (min). At steady state ( $dC/dt$ ) $V = 0$ ,  $C = C_{out}$ ,  $Q_{in} = Q_{out} = 100$  mL/min,  $C_{in} = 1.04 \times 10^{-2}$  mM,  $C_{out} = 9.72 \times 10^{-3}$  mM,  $V = 1.67$  L

$$k = 4.19 \times 10^{-3} \text{ min}^{-1}$$

### C-3. Removal Efficiency

For HC system (Batch Reactor), percent removal of rhodamine B within 100 min were calculated as follow:

$$\% \text{ Removal} = \frac{C_o - C_t}{C_o} = 1 - \frac{C_t}{C_o} \quad (\text{at } t = 100 \text{ min}) \quad (\text{Eq. C - 2})$$

where  $C_o$  = initial dye concentration (mM) in HC system;  $C_t$  = dye concentration at time  $t = 100$  min (mM).  $C_t/C_o$  for Venturi tubes were obtained from the exponential regression equations:

- Venturi tube 1 (Model 283) with initial concentration of  $2.51 \times 10^{-3}$  ( $1.45 \times 10^{-3}$  measured value),  $C_t/C_o = 1.01e^{-0.00114t}$  ( $t = 0-100$  min),  $R^2 = 0.985$ ;
- Venturi tube 1 (Model 283) with initial concentration of  $1.20 \times 10^{-2}$  ( $9.49 \times 10^{-3}$  measured value),  $C_t/C_o = 1.01e^{-0.000531t}$  ( $t = 0-100$  min),  $R^2 = 0.966$ ;
- Venturi tube 2 (Model 287) with initial concentration of  $1.20 \times 10^{-2}$  ( $8.74 \times 10^{-3}$  measured value),  $C_t/C_o = 1.00e^{-0.00109t}$  ( $t = 0-100$  min),  $R^2 = 0.978$ ;

For AC system (Completely Mixed Flow-through System), removal efficiency was calculated as follow:

$$\% \text{ Removal} = \frac{C_o - C_{ss}}{C_o} \quad (\text{Eq. C - 3})$$

where  $C_o$  = initial dye concentration in US reactor (mM);  $C_{ss}$  = dye coccentration at steady state (dye concentration after 48 min in our case) (mM). According to C-2,  $C_o = C_{in} = 1.04 \times 10^{-2}$  mM,  $C_{ss} = C_{out} = 9.72 \times 10^{-3}$  mM.

$$\% \text{ Removal} = 6.54 \%$$

### C-4. Energy Efficiency Calculation of HC and AC processes

Energy efficiency for HC system:

$$= \frac{\text{Total rhodamine B removed (mmole)}}{\text{Energy input (J)}} = \frac{(C_o - C_t) \cdot V}{W \cdot t}$$

where  $C_o$  = initial dye concentration (mM) in HC system;  $C_t$  = dye concentration at time  $t = 100$  min (mM);  $V$  = total volume of solution (L);  $W$  = sum of power rate of all involved equipment (Watt);  $t$  = operation time (100 min in our case) (s). According to Eq. C-3,  $C_o - C_t = (\% \text{ Removal}) \cdot C_o$ .

For Venturi tube 1 (Model 283) with initial concentration of  $2.51 \times 10^{-3}$  ( $1.45 \times 10^{-3}$  measured value)

$$= \frac{1.45 \times 10^{-3} \text{ mmol/L} \times 2.50 \text{ L} \times 9.88 \%}{138 \text{ Watt} \times 100 \text{ min} \times 60 \text{ s/min}} = 4.33 \times 10^{-10} \text{ mmol/J}$$

For Venturi tube 1 (Model 283) with initial concentration of  $1.20 \times 10^{-2}$  ( $9.49 \times 10^{-3}$  measured value)

$$= \frac{9.49 \times 10^{-3} \text{ mmol/L} \times 2.50 \text{ L} \times 4.22 \%}{138 \text{ Watt} \times 100 \text{ min} \times 60 \text{ s/min}} = 1.21 \times 10^{-9} \text{ mmol/J}$$

For Venturi tube 2 (Model 287) with initial concentration of  $1.20 \times 10^{-2}$  ( $9.49 \times 10^{-3}$  measured value)

$$= \frac{8.74 \times 10^{-3} \text{ mmol/L} \times 2.50 \text{ L} \times 10.33 \%}{138 \text{ Watt} \times 100 \text{ min} \times 60 \text{ s/min}} = 2.73 \times 10^{-9} \text{ mmol/J}$$

Energy efficiency for AC system:

$$= \frac{\text{Total rhodamine B removed (mmole)}}{\text{Energy input (J)}} = \frac{(C_o - C_{ss}) \cdot V}{W \cdot t} = \frac{(C_o - C_{ss}) \cdot Q}{W}$$

where  $C_o$  = initial dye concentration (mM) in HC system;  $C_{ss}$  = dye concentration at steady state (mM);  $Q$  = Flow rate (L/s);  $W$  = sum of power rate of all involved equipment (Watt).

Energy efficiency for AC system

$$= \frac{(C_o - C_{ss}) \cdot Q}{W} = \frac{(1.04 \times 10^{-2} - 9.72 \times 10^{-3}) \text{ mmol/L} \times 100 \text{ ml/min}}{(550 \times 70 \%) \text{ Watt} + 75 \text{ Watt}}$$

$$= 2.46 \times 10^{-9} \text{ mmol/J}$$